Integrated tectonic basin modelling as an aid to understanding deep-water rifted continental margin structure and location

Alan M. Roberts[1]*, Nick J. Kusznir[2], Richard I. Corfield[3], Mark Thompson[3] and Richard Woodfine[3]

[1]*Badley Geoscience Ltd, North Beck House, North Beck Lane, Spilsby, Lincolnshire, PE23 5NB, UK*
[2]*University of Liverpool, Department of Earth & Ocean Sciences, Liverpool L69 3BX, UK*
[3]*BP Exploration Operating Co. Ltd, Chertsey Road, Sunbury on Thames, Middlesex TW16 7LN, UK*
**Corresponding author (e-mail: alan@badleys.co.uk)*

ABSTRACT: An integrated workflow has been devised for the investigation of deep-water rifted continental margins. At a margin this allows us to predict the crustal structure, the distribution of continental-lithosphere thinning and the location of the ocean–continent transition with a new degree of confidence. The workflow combines the analytical techniques of 2D or 3D gravity inversion, 2D or 3D flexural backstripping with reverse thermal subsidence modelling, upper-crustal fault analysis and rifted margin forward modelling. No one technique on its own can provide all of the required answers, nor can it provide answers without some degree of uncertainty. The use of a combination of techniques, however, provides answers to several different problems and, crucially, more confidence in these answers.

The workflow provides direct information on the present-day geometry of rifted margins and leads towards a better understanding of the geodynamic evolution of these margins. It also provides information which can inform the exploration process by making predictions about crustal structure at the ocean–continent transition, the location of the continent–ocean boundary, stretching-factor, heat-flow magnitude and history, palaeobathymetric history and subsurface palaeostructure. Application of the workflow is illustrated here with reference to the continental margins of West India, Brazil, West Australia, Norway and Newfoundland–Iberia.

INTRODUCTION

Deep-water rifted continental margins are now a major focus for oil and gas exploration. Crucial to planning an exploration strategy in such areas is the need to understand crustal structure within the ocean–continent transition, both at the present day and its evolution through time. Where wide-angle refraction data or deep-seismic reflection data are available, offering deep imaging and velocity control, some constraints on present-day crustal structure can be interpreted directly (e.g. Funck *et al*. 2003; Contrucci *et al*. 2004; Hopper *et al*. 2007; Collier *et al*. 2009; Shillington *et al*. 2009). Good quality wide-angle or deep-reflection data are, however, often unavailable and so we must gain our understanding of the structure and structural evolution indirectly, using geological/geophysical observations as input to models which predict the crustal structure. The subsidence record of the sediments overlying present-day margins offers a particularly important constraint to such models, being in general the only readily available geological dataset at deep-water margins, which with simple isostatic assumptions can offer constraints on crustal structure both now and in the past. Another important dataset is the present-day gravity-anomaly field, which can be combined with simple stratigraphic information to provide constraints on present-day crustal structure.

Through the course of a number of exploration-focused case studies, across margins world-wide, we have used tectonic-basin modelling techniques to help us:

- map the present-day crustal-basement thickness across the margin, including prediction of depth to Moho;
- map beta-factors/thinning factors associated with margin break-up, leading to prediction of heat-flow history;
- identify (i) areas of stretched continental crust, (ii) areas of highly attenuated continental crust within the ocean–continent transition (OCT), (iii) the location of the continent–ocean boundary (COB), (iv) areas of oceanic crust;
- assess the likely impact of volcanic addition during break-up (decompression melting) on predictions of crustal thickness and beta/thinning factor;
- model the subsidence history of the margin and predict its palaeobathymetric evolution.

Assembling this information has helped us to understand the crustal geometry and the geological evolution of deep-water rifted margins.

There is, however, no one single modelling technique that can provide all of the required geological answers, nor can a single modelling technique provide answers without some degree of uncertainty. Instead, we have put together a multi-technique workflow, the results from which integrate to provide the required answers. By tackling the same geological problem in more than one way the integrated workflow also provides increased confidence in these answers. The aim of this paper is to describe the components of the workflow and illustrate them with examples from case studies.

Petroleum Geoscience, Vol. **19**, 2013, pp. 65–88
DOI: 10.1144/petgeo2011-046

Table 1. *Summary of the integrated workflow showing the methods used, data requirements and general availability, the principal output and results, how calibration is achieved and the principal uncertainties at each stage*

Workflow technique*	Data input required	Principal output/results	Calibration	Principal uncertainties
2D/3D gravity inversion, with lithosphere thermal gravity anomaly correction	Free-air satellite gravity anomaly[1] Bathymetry 2D/3D[1] Sediment thickness 2D/3D[1 or 2] Ocean isochrons[1] and/or rift/break-up age[1]	Depth to Moho, present-day Crustal thickness, present-day Stretching/thinning factor, leading towards heat-flow prediction OCT/COB location	Seismic constraints on Moho depth/crustal thickness/volcanic addition Predictions must honour geological constraints	Reliability of sediment thickness Influence of dynamic topography on reference crustal thickness
2D/3D post-break-up flexural backstripping	Bathymetry[1] Stratigraphic depth model[2] Lithological information by layer[1 or 2] Rift/break-up age[1] Map of beta-factor (3D only)[2]	Stretching/thinning factor (from 2D) Post-rift palaeobathymetry history Post-rift palaeostructure history	Palaeobathymetry markers within backstripped stratigraphy Predictions must honour geological constraints	Reliability of depth model Deep-water palaeobathymetric constraints
2D/3D syn- & post-kinematic flexural backstripping	Bathymetry[1] Depth model to base syn-rift/top basement[2] Rift/break-up age[1]	Stretching/thinning factor, leading towards heat-flow prediction Crustal thickness, present-day OCT/COB location Post-rift palaeobathymetry history	Seismic constraints on Moho depth/crustal thickness/volcanic addition Predictions must honour geological constraints	Seismic imaging of base syn-rift/top basement Depth conversion of deep stratigraphy
Quantifying upper-crustal fault extension (2D)	Cross-section/seismic profile with detailed fault interpretation[1 or 2]	Fault-controlled structural model Upper-crustal stretching factor Footwall-uplift estimates	Calibrated by input section Can be compared with 2D backstripping results	Seismic imaging of complex fault geometries
Forward modelling kinematics of break-up (2D)	Target regional cross-section[1 or 2] Outline rift/break-up history[1 or 2] Faulting constraints on magnitude of stretching/thinning[2]	Crust & lithosphere cross-sections Rift to break-up evolution Stretching/thinning factor Predicted heat-flow and subsidence history	Gravity/bathymetry match Can be calibrated against 2D backstripped water-loaded subsidence and crustal thickness	Modelling is complex, so difficult to define unique solution

*2D section-based, 3D map-based
[1]available in public domain
[2]normally proprietary information

THE INTEGRATED WORKFLOW

There follows here a brief description of the full workflow, subsequent to which follows a more complete description of each technique together with illustration and discussion of the output. A summary of the workflow is provided in Table 1. This highlights data requirements and general availability, the principal output and results, how calibration is achieved and the principal uncertainties at each stage of the workflow.

- **2D/3D gravity inversion.** Key to the gravity inversion method used (Greenhalgh & Kusznir 2007; Alvey *et al*. 2008; Chappell & Kusznir 2008) is the incorporation of both a lithosphere thermal gravity-anomaly correction, addressing the elevated post-break-up lithosphere geotherm, and a prediction of the amount of new volcanic crustal-addition at high stretching factors. This allows us to predict (i) depth to Moho, (ii) thickness of residual continental-crustal basement, (iii) the structure of the OCT, (iv) location of the COB, incorporating the continental lithosphere's first-order responses to extreme thinning in the predictions.
- **2D/3D post-break-up flexural backstripping.** The established technique of post-rift flexural backstripping, incorporating reverse thermal-subsidence modelling (Kusznir *et al*. 1995; Roberts *et al*. 1998, 2009), is used to quantify the long-term post-break-up subsidence history of continental-margin lithosphere. This allows us to predict the spatially varying magnitude of the whole-lithosphere thermal anomaly and stretching factor resulting from the break-up process, together with the post-break-up palaeobathymetric evolution of the margin. It is a simple but powerful technique to employ as the fundamental requirement is simply a 2D or 3D model (cross-section or maps) of the post-break-up margin stratigraphy.
- **2D/3D syn-kinematic flexural backstripping.** Post-break-up backstripping is, indeed, a straightforward technique to employ, but, at many margins, the stratigraphical location of the base of the post-break-up sequence may be uncertain or unknown, particularly at margins where mobile salt is involved. In such cases, however, the base of the syn-break-up sequence (or top basement) may be more easily identified. Where the base of the syn-break-up sequence is known, backstripping to reveal syn-plus-post-break-up water-loaded subsidence allows us to use a modified version of the McKenzie (1978) subsidence model to convert backstripped water-loaded subsidence to estimates of lithosphere stretching/thinning factor. The conversion of subsidence to stretching incorporates the isostatic consequences of syn-break-up volcanic addition (underplating, intrusion), a process which in turn leads to the formation of new ocean crust. From this we can map crustal basement thicknesses and the OCT in a comparable (but independently constrained) way to the output from the gravity inversion method.
- **Quantifying upper-crustal fault extension.** Gravity and subsidence modelling aim to quantify extension of the whole crust and/or lithosphere. We believe, however, that the process of depth-dependent lithosphere stretching/thinning

during break-up (Roberts *et al*. 1997; Davis & Kusznir 2004; Kusznir *et al*. 2004) means that upper-crustal extension need not necessarily balance these estimates of deeper-seated stretching and thinning. It is, therefore, important to quantify fault-controlled upper-crustal extension either by forward modelling or section restoration. This provides information about the partitioning of extension through the crust, which ultimately impacts upon the predictions of the top basement heat-flow model (Kusznir *et al*. 2005).

- **Forward modelling the kinematics of break-up.** Finally we aim to bring together the complete rifting/break-up process within a single forward kinematic model, built upon earlier work by Kusznir *et al*. (2005) and Kusznir & Karner (2007), incorporating observations from the previous analyses in its construction. The forward model of full (conjugate) margin structure is calibrated against present-day bathymetry and gravity measurements and/or backstripped water-loaded subsidence. It is used not just to predict the crustal structure and evolution of the margin, but also the time-dependent heat-flow history, controlled by the kinematics of the break-up process.

It is important to emphasize, however, that through most of the workflow (with the exception of the final forward modelling) we are not attempting to model or explain the explicit geodynamic processes of continental break-up. Rather, we prefer our analytical techniques to remain, as much as is possible, model-independent in the context of break-up processes. Our primary objective, in an exploration context, is to predict present-day crustal geometries and margin configuration, plus the associated cumulative stretching/thinning factors and heat-flow consequences. Having done this we might then wish to speculate about the break-up process itself using, for example, the models of Kusznir & Karner (2007) or Huismans & Beaumont (2008, 2011), but we believe that it is important first to understand the present-day first-order crustal geometries and then from this move to draw further inferences about processes or apply further modelling. It is inadvisable to make assumptions about break-up processes before the first-order crustal geometry has been investigated.

2D/3D GRAVITY INVERSION

Gravity inversion is an excellent entry point into the analysis of rifted continental margins because (i) the details of the stratigraphic information required to support the analysis are less than those required by some of the other methods described later, thus the study can be started early in the exploration process, and (ii) much of the required input information is publically available via the internet (Table 1).

The gravity inversion method used follows that described in detail by Greenhalgh & Kusznir (2007), Chappell & Kusznir (2008) and Alvey *et al*. (2008). The inversion scheme uses three principal sets of input data:

- satellite free-air gravity anomaly data, typically Sandwell & Smith (1997, 2009);
- bathymetric/topographic data, typically IOC, IHO, BODC (2003);
- information on total sediment thickness (seabed to top basement) and bulk lithology of the stratigraphic interval.

The former two are publically available, whereas, although sediment thickness information can be obtained from public sources (Divins, NGDC 2009), more reliable sediment thickness information is normally obtained from focused proprietary study of seismic reflection data and supporting stratigraphic information and so should be used if available.

The principal output from gravity inversion at rifted margins comprises maps of:

- depth to Moho (present day);
- total crustal basement thickness (continental or oceanic);
- residual (present-day remaining) thickness of continental crustal basement;
- total stretching factor (β) and thinning factor (γ) across the margin, where $\gamma=1-1/\beta$.

In addition, cross-sections of whole-crustal geometry can be extracted from these maps and the maps of stretching/thinning factor can be readily converted to maps of top basement heat-flow.

The gravity inversion methodology and workflow is summarized in Figure 1a (adapted from Alvey 2010). Key to the success of the gravity inversion method are two geological corrections, made in order to account for the highly attenuated nature of the continental crust at rifted margins. The two corrections are linked to each other by thinning factor and are described in detail by Chappell & Kusznir (2008).

- A correction is made for the lithosphere thermal gravity anomaly associated with the elevated geotherm resulting from rifting/break-up of the margin. At the time of break-up this may be as much as −350 mgal at the spreading centre itself (Chappell & Kusznir 2008, figs 2, 4). The negative anomaly will be of lower magnitude, but still significant, within the attenuated lithosphere of the adjacent continental margin. The magnitude of the gravity anomaly decreases with time as the lithosphere cools following break-up, thus it is important to know the age of break-up in order to constrain the magnitude of the present-day lithosphere thermal gravity anomaly. The thermal gravity anomaly is calculated using the premise of the McKenzie (1978) uniform-stretching model.
- A correction is made for volcanic/magmatic addition to the crust at high stretching factors. Following McKenzie & Bickle (1988) and White & McKenzie (1989), we assume that decompression melting of the lithosphere occurs at high stretching factors, resulting in magmatic addition to the total thickness of the crust (Chappell & Kusznir 2008, fig. 3). In simple terms, as stretching proceeds beyond a given critical value the original continental crust will continue to stretch and thin, but the total thickness of the crust will be buffered by the addition of new magmatic material. Traditionally this might be regarded as underplating of the outer margin, although we imply no specific mechanism or location for the melt. Thus, following magmatic addition, the location of the base of the crust is controlled both by the magnitude of crustal stretching/thinning and by the amount of newly added magmatic material.

Constraining both the magnitude of the lithosphere thermal gravity anomaly and the amount of magmatic addition to the crust is dependent on knowing the lithosphere stretching factor; thus, within the gravity inversion scheme there is a feedback loop between all three variables.

Before illustrating some results of the gravity inversion method it is worth considering and illustrating how magmatic addition to the crust is parameterized during stretching/thinning leading to break-up, as the same parameterization is returned to later when we consider the 'syn-kinematic flexural backstripping' method. Figure 1b is adapted from Chappell & Kusznir (2008, fig. 3d), which in turn is based on the results of McKenzie & Bickle (1988) and White & McKenzie (1989). Its shows how magmatic addition to the crust is assumed to occur for two distinct lithosphere conditions. For normal temperature mantle, melting begins at a critical thinning factor of ~0.7. Melt continues to be generated as stretching/thinning proceeds until ~7 km of melt has been produced when the thinning factor reaches 1.0. At this point the continental crust is completely attenuated and ~7 km of new volcanic oceanic crust remains. This is the typical circumstance of a 'normal' continental

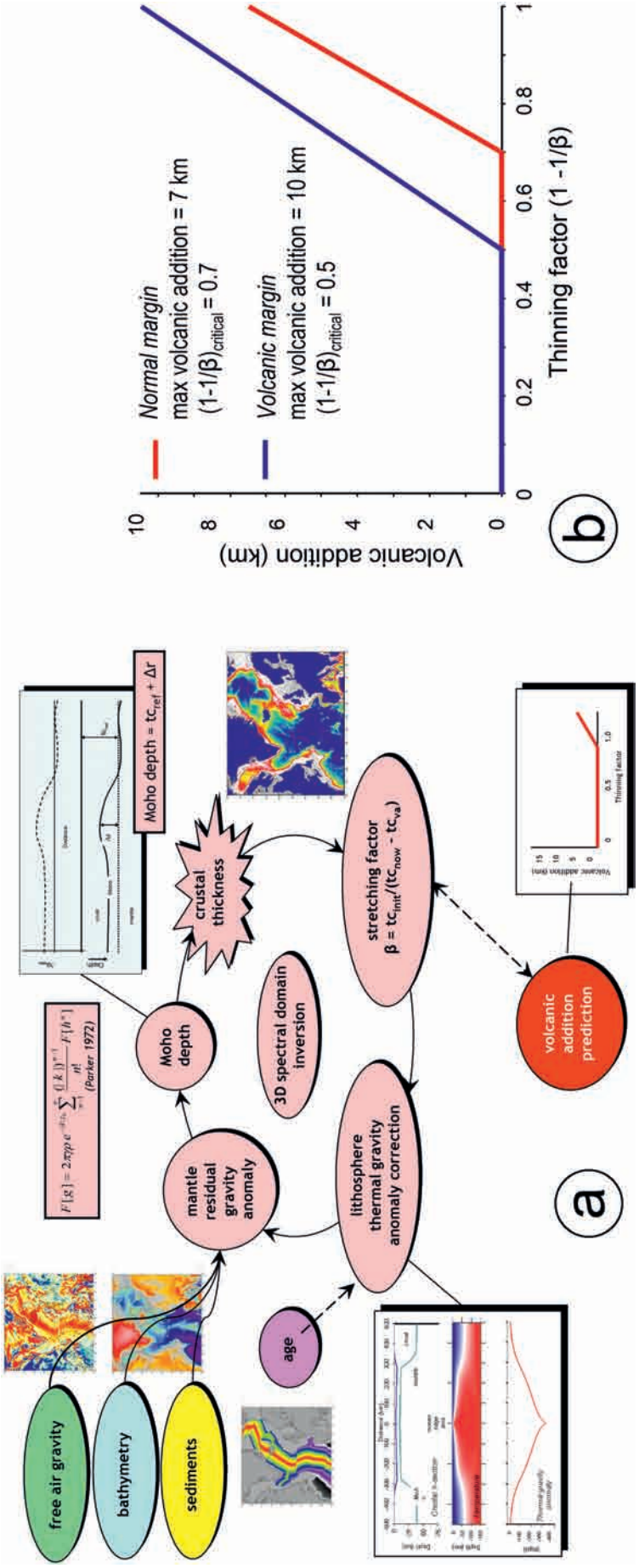

Fig. 1. (**a**) Schematic outline of gravity inversion methodology to determine Moho depth, crustal-basement thickness and continental-lithosphere thinning factor, using gravity-anomaly inversion incorporating a lithosphere thermal gravity anomaly correction and decompression melt prediction. Adapted from Alvey (2010). (**b**) Parameterization of the decompression melting model of White & McKenzie (1989) to predict melt thickness (volcanic addition) as a function of thinning factor at a 'normal' rifted margin and at a 'volcanic' rifted margin. The onset of melting begins at critical thinning factors of 0.7 and 0.5, respectively. Thinning factor = 1 defines the formation of new oceanic crust (no continental crust or lithosphere remaining). Adapted from Chappell & Kusznir (2008).

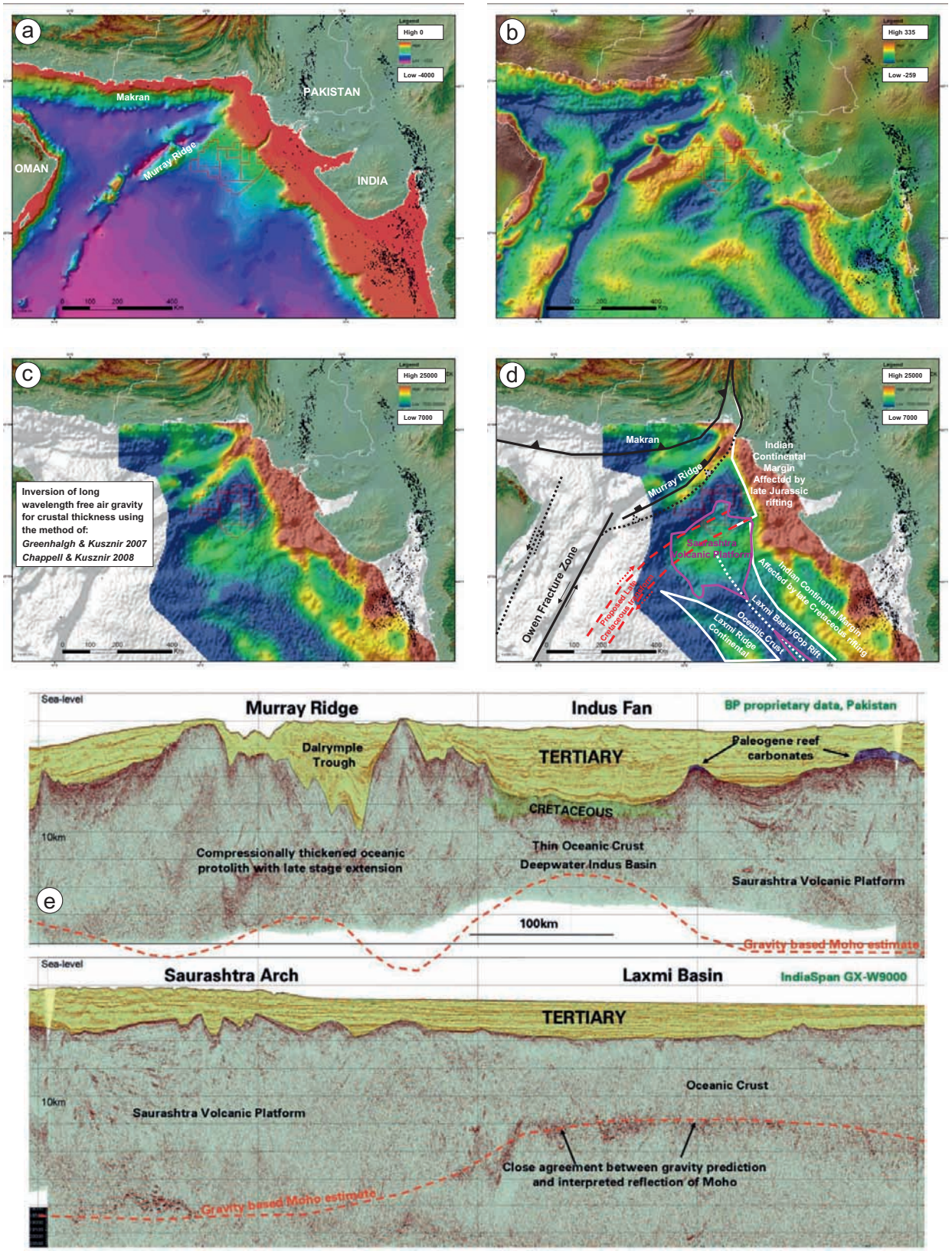

Fig. 2. (**a**) Bathymetry (m) (IOC, IHO, BODC 2003) and topography (SRTM, Farr *et al*. 2007) for the NW India volcanic continental margin. (**b**) Satellite free-air gravity anomaly (offshore, mgal) for the NW India margin (Sandwell & Smith 1997). (**c**) Map of present-day (offshore) crustal thickness (continental and oceanic, m) produced using the gravity inversion technique of Greenhalgh & Kusznir (2007), Chappell & Kusznir (2008) and Alvey *et al*. (2008), applying the volcanic addition correction for a 'volcanic' margin (Fig. 1) at a break-up age of 80 Ma. (**d**) Map of crustal thickness overlaid by an interpretation of the major structural elements picked out by the map. Note the interpretation of low-thickness crust (~7 km) in the Laxmi Basin as likely to be oceanic. (**e**) Overlay of Moho depth determined from gravity inversion on to a composite seismic depth section, showing good agreement between gravity and seismic reflection depth estimates across the Laxmi Basin and Saurashtra Platform (from Corfield *et al*. 2010, seismic originally courtesy of BP and ION-GXT). Reproduced courtesy of GX Technology.

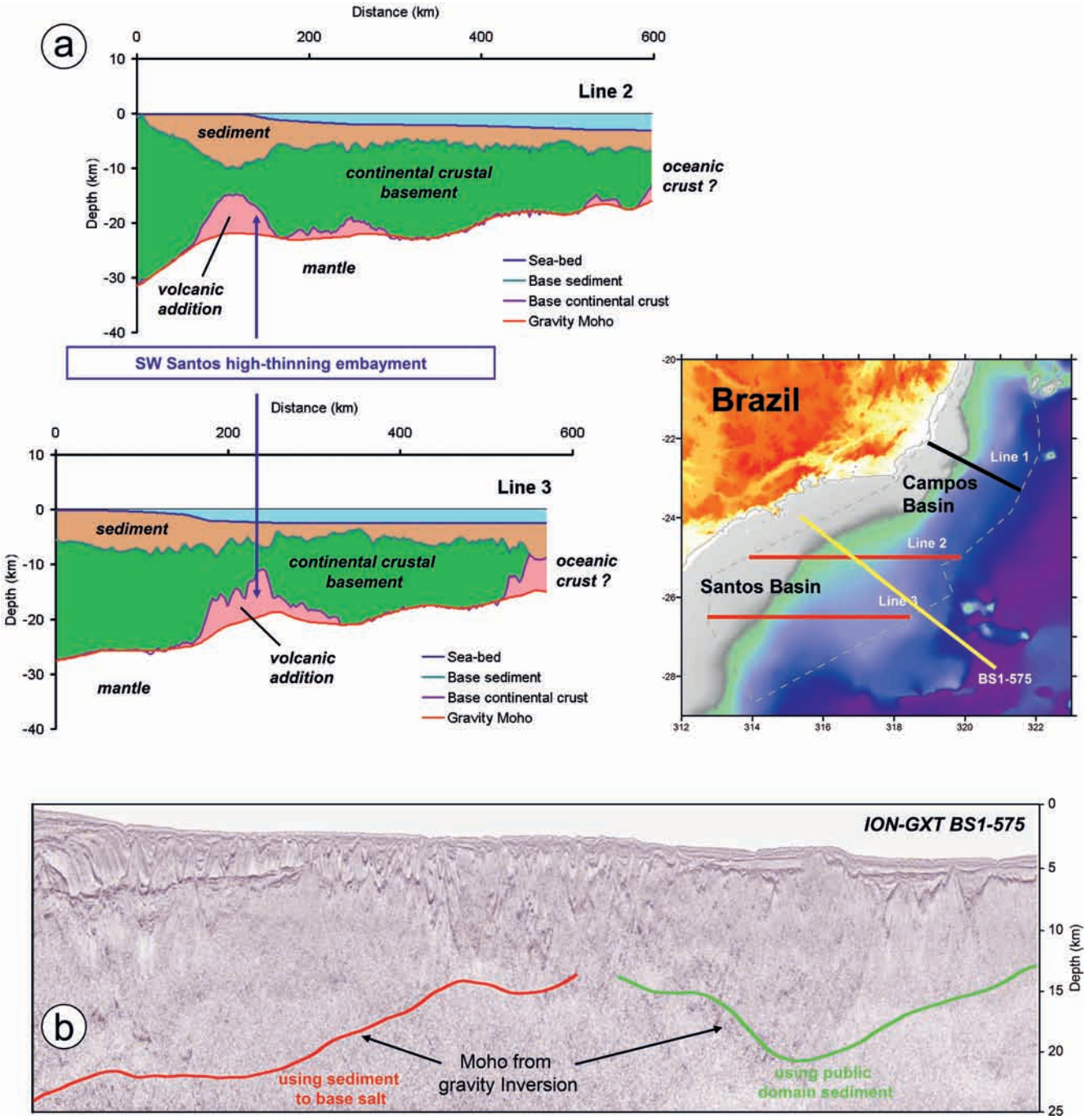

Fig. 3. (**a**) Two crustal cross-sections derived and extracted from a full 3D gravity inversion of the Santos and Campos Basins Atlantic margin, offshore Brazil (identified on the inset map as Lines 2 & 3). The sections are a composite of two inversion runs: (i) in the east the sections are constructed from an inversion using the volcanic-addition parameters of a 'normal' rifted margin (Fig. 1); (ii) in the west the sections are constructed from an inversion using the volcanic-addition parameters of a 'volcanic' rifted margin (Fig. 1). Volcanic addition on the sections is an illustration of the predicted total thickness of melt addition, shown for graphical convenience as an underplating geometry. Note the presence of the highly thinned Santos embayment on both sections. Line 1 on the inset map shows the regional location of Figure 6. (**b**) Overlay of Moho depth determined from gravity inversion on to pre-stack, depth-migrated, deep-seismic reflection section BS1-575 running NW to SE across the Sao Paulo Plateau (see inset map for location, seismic courtesy of ION-GXT). Sediment thicknesses used in the gravity inversion were from BP for the NW part of the line while public domain sediment thickness estimates were used to the SE.

margin where the thickness of oceanic crust immediately outboard of the COB corresponds to the global average. If the mantle temperature is raised by ~100°C, melting models show that the critical thinning factor at which melting of the lithosphere begins is lowered to ~0.5. From this point melt is added to the crust until the thinning factor reaches 1.0, at which point ~10 km of new volcanic addition is assumed to have occurred. This is the circumstance for a 'volcanic' continental margin associated with the production of overthickened oceanic crust.

The gravity inversion scheme can incorporate both of these melting parameterizations in its calculations (or, indeed, any combination of critical thinning factor and maximum melt

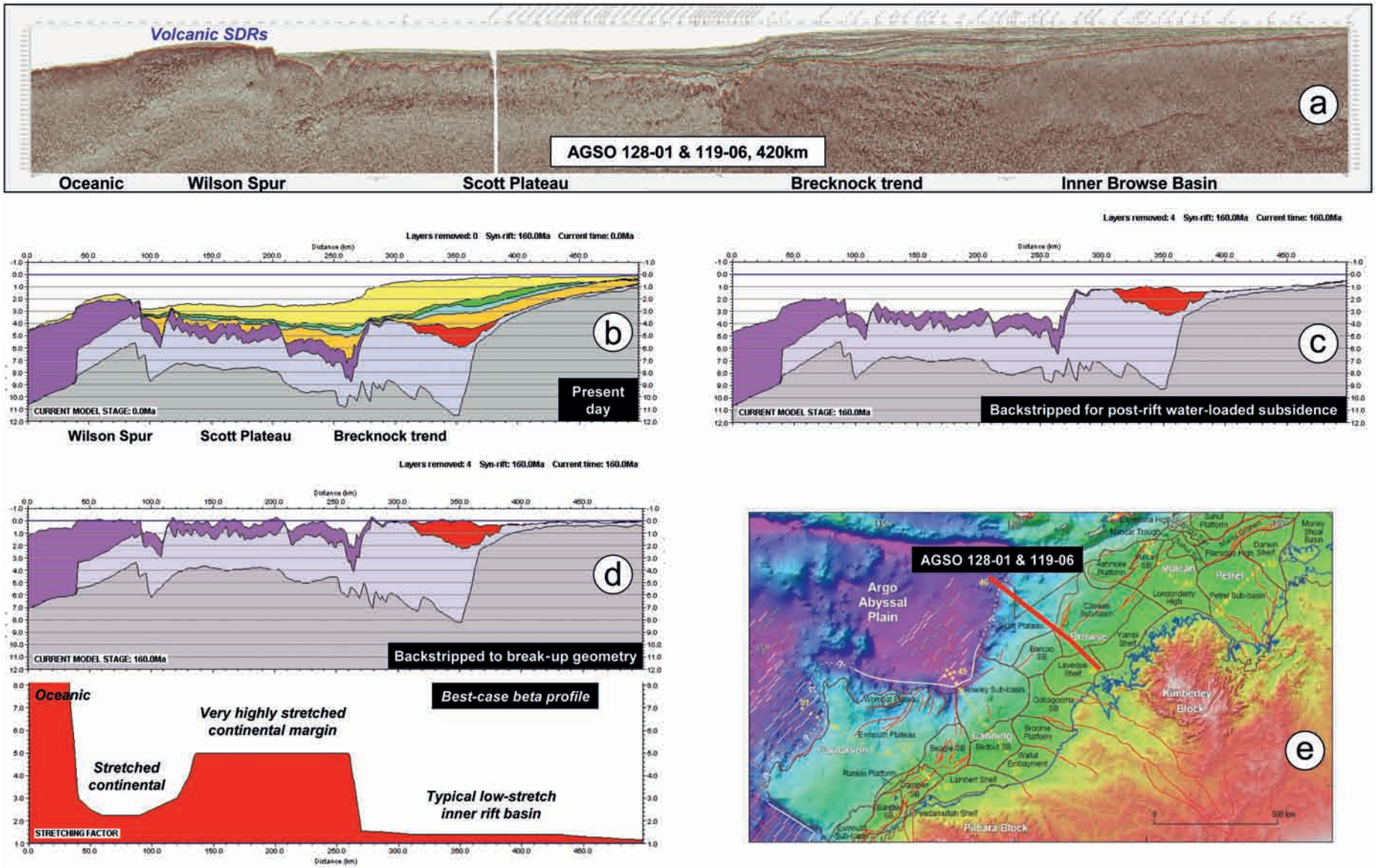

Fig. 4. 2D post-break-up flexural backstripping of a regional transect across the Browse Basin continental margin, NW Australia. (**a**) Composite regional seismic depth profile (2 lines) extending from close to the Australian coast in the SE to the edge of the Argo oceanic abyssal plain in the NW [located in (e)]. © Commonwealth of Australia (Geoscience Australia) 2011. The interpretation shows a set of horizons covering the Jurassic–seabed interval (previous published interpretations are referenced in the text). (**b**) Depth section prior to backstripping. Key stratigraphic intervals are (i) syn-rift/break-up extrusive basalts in dark purple, (ii) the time-equivalent Callovian syn-rift sediments in red, both the basalts and Callovian are assigned a top-surface age of 160 Ma, (iii) a thick Triassic section in light purple, extending to top basement (grey) and associated with a prior Triassic rift event. (**c**) Flexurally backstripped to 160 Ma (Te 3 km) with no reverse thermal-subsidence modelling applied. There is a residual bathymetry of ~2 km above the Wilson Spur, ~3 km above the Scott Plateau, ~1 km above Brecknock, at a time when each of these areas should be at/close to sea-level. (**d**) Flexurally-backstripped to 160Ma (Te 3 km) with reverse thermal-subsidence modelling applied, controlled by the best-case beta profile below the section. The Wilson Spur, Scott Plateau and Brecknock are all restored to their preferred sea-level datum by applying the highly laterally-variable thermal subsidence model. (**e**) Location map for the NW Australian coast, the offshore basins and the seismic profile described (after Goncharov 2004).

thickness). The end-member circumstance of no magmatic addition during stretching can also be invoked if we wish to consider a 'magma-poor' margin, such as that described in Newfoundland and Iberia (Whitmarsh *et al*. 2001).

West Indian volcanic continental margin

Figure 2 shows the gravity inversion method applied to the West Indian volcanic continental margin (Roberts 2008). Figure 2a shows bathymetry (IOC, IHO, BODC 2003) and topography (SRTM, Farr *et al*. 2007) for the margin, while Figure 2b shows a map of satellite free-air gravity anomaly (Sandwell & Smith 1997). These two primary data sources have been combined with the BP model for sediment thickness on the margin (not illustrated) and input to the gravity inversion scheme.

Figure 2c shows the best-case map of present-day crustal basement thickness, produced with the following control parameters for the inversion:

- break-up age 80 Ma (this is a simplifying approximation of a complex multi-phase break-up history (Corfield *et al*. 2010));
- reference Moho depth and initial crustal thickness 35 km;
- critical thinning factor 0.5, with maximum volcanic addition 10 km ('volcanic' continental margin).

Crustal basement thickness on this map includes volcanic contributions to the total crustal thickness, i.e. it includes the thickness of any oceanic crust present, not just the thickness of the residual continental crust. Although not illustrated in this example, it is very straightforward to produce a map of gravity-derived beta-factor/thinning factor once the present-day basement crustal thickness and an estimate of original crustal thickness are known.

Figure 2d shows the same map of crustal basement thickness, overlaid with an interpretation of the major structural elements picked out by the map (e.g. Talwani & Reif 1998; Daley & Alam 2002; Krishna *et al*. 2006; Roberts 2008; Corfield *et al*. 2010). Perhaps most interesting in this regional geological interpretation is the separation of the Laxmi Ridge continental block from the mainland India continental margin by the Laxmi Basin, which has a uniform crustal thickness of ~7 km, compatible with the presence of normal thickness oceanic crust between two continental blocks (see also Talwani & Reif 1998). This illustrates how the gravity inversion method can be used as the first step in defining the continental/oceanic geometry of a complex rifted margin. Corfield *et al*. (2010) have demonstrated the success of this model (Fig. 2e) by showing that the Moho predicted by the gravity inversion matches closely the seismic Moho interpreted on deep reflection data across the Laxmi Basin and Saurashtra Platform.

Santos Basin, Brazil

The gravity inversion method is fundamentally a map-based 3D method, but it is often revealing to extract 2D cross-sections of predicted crustal geometry from these maps. Figure 3a shows two composite W–E cross-sections extracted from a gravity inversion of the Santos Basin, offshore east Brazil (e.g. Davison 1999; Karner & Driscoll 1999*a*; Mohriak *et al*. 2008). The cross-sections have been produced by merging the results of two separate inversion runs, based once more on bathymetric data from IOC, IHO, BODC (2003), satellite free-air gravity data from Sandwell & Smith (1997) and BP proprietary data for total sediment thickness across the basin. The initial reference crustal thickness was 35 km and the break-up age 115 Ma.

In the east the two cross-sections are based on a gravity inversion assuming the conditions of a 'normal' continental margin, critical thinning factor of 0.7 and maximum magmatic addition of 7 km. Whereas in the west, where a volcanic province with extrusive seaward-dipping reflectors (SDRs) has been recognized north of the Florianopolis Fracture Zone (Mohriak *et al*. 2008), the gravity inversion has assumed the conditions of a 'volcanic' continental margin with vigorous magmatic addition, critical thinning factor of 0.5 and maximum magmatic addition of 10 km.

The two cross-sections show in their upper part, as input to the model, the depth of the water layer and the thickness of the total-sediment layer down to top basement. Below this is the predicted thickness of the remaining thinned continental crust plus the predicted thickness of volcanic addition, created by decompression melting during stretching/break-up. For display purposes we show this volcanic addition accreted to base of the continental crust as magmatic underplating, although some of it would take the form of extrusives above thinned continental crust.

In the east the northern line is predicted to terminate still within attenuated continental crust, while the southern line reaches oceanic crust of 7 km thickness. Perhaps more interesting though, is the area of the inner Santos Basin further to the west in which an embayment of significant volcanic addition is predicted on both cross-sections. This area of volcanic addition lies immediately to the north of a possible oceanic embayment associated with extrusive volcanics and a possible failed spreading centre (the Abimael Ridge), previously recognized by Scotchman *et al*. (2006, 2010) and Mohriak *et al*. (2008). The prediction of significant volcanic addition and highly attenuated crust on both sections is fully compatible with this conclusion.

Figure 3b shows the Moho determined from gravity inversion superimposed on the ION-GXT BS1-571 pre-stack depth-migration seismic section. The Moho from gravity inversion and that interpreted from the seismic reflection data show similar geometries and trends. The combined use of gravity inversion and deep, long-offset seismic reflection data shows the transition from thinned continental crust under the Sao Paulo Plateau in the NW to transitional crust in the SE.

2D/3D POST-BREAK-UP FLEXURAL BACKSTRIPPING

2D post-rift/post-break-up flexural backstripping uses the established method of Kusznir *et al*. (1995) and Roberts *et al*. (1998) to reverse-model the thermal subsidence history of rift basins and rifted margins along chosen 2D transects. In so doing it produces a series of isostatically balanced cross-section restorations, predicting palaeobathymetry and palaeostructure through time. The method has been applied previously in a number of published case studies across rifted margins (e.g. Roberts *et al*. 1997; Baxter *et al*. 1999; Clift *et al*. 2002; Davis & Kusznir 2004; Kusznir *et al*. 2004, 2005; Green *et al*. 2009), but is illustrated here with reference to a previously unpublished example across the Browse Basin continental margin of NW Australia.

Browse Basin, NW Australia

Figure 4a shows composite regional seismic line AGSO 119–06 & 128–01 across the Browse Basin continental margin. Figure 4b shows a depth model of this section. The line is ~500 km in length and extends from oceanic crust of the Argo abyssal plain in the NW to the inner part of the Browse Basin, close to the coast, in the SE. This line, being of particularly excellent length and quality, has been previously illustrated and interpreted in a number of publications (Symonds *et al*. 1994, 1998; Struckmeyer *et al*. 1998; Goncharov 2004; Hoffman & Hill 2004).

We illustrate here how post-rift/post-break-up flexural backstripping, with reverse thermal subsidence modelling, can be used to derive an estimate of beta stretching factors across this profile and from this gain some insight into the dynamics of the rifting and break-up process. Break-up of the margin and formation of the Argo oceanic crust is thought to have occurred at 158–155 Ma (Symonds *et al*. 1998). We perform backstripping to an age of 160 Ma, which we take to be the end of the fault-controlled rift episode and the onset of thermal subsidence during the seafloor spreading.

Backstripping of the section has been performed assuming that there are three palaeobathymetric sea-level markers of Jurassic rift/break-up age across the section, each of which should be restored back to sea-level at 160 Ma in any successful restoration.

- The major tilted fault-blocks of the Brecknock trend are capped by classic footwall uplift unconformities (Yielding & Roberts 1992), diagnostic of fault-block emergence during the Jurassic rift phase.
- Syn-rift/break-up basalts have been penetrated in the outer basin area of the Scott Plateau (e.g. the Maginnis-1 well, 2003), which Symonds *et al*. (1998) interpreted to have been extruded either as sub-aerial flows or in a shallow-marine environment, as part of a major volcanic province, during the Middle Jurassic.
- Immediately inboard of the Argo oceanic crust lies the bathymetrically-high block of the Wilson Spur. The Wilson Spur is capped by volcanic SDRs (Symonds *et al*. 1998), which in turn are capped by a pronounced truncating erosional unconformity, indicating emergence after extrusion of the basalts.

In addition the area inboard of the Brecknock trend contains shallow-marine sediments of Middle Jurassic age which provide an additional palaeobathymetric constraint on the Jurassic restoration.

Backstripping with reverse thermal-subsidence modelling incorporates the reverse-modelling of three first-order geological processes, in order to provide a restoration sequence through the post-rift history. These are (i) layer-by-layer removal of the stratigraphy with flexural-isostatic compensation for the removal of the loads, (ii) decompaction of the underlying stratigraphy as the overlying loads are removed, (iii) reverse modelling the thermal cooling of the lithosphere (i.e. heating up back through time) in order to compensate for the thermal subsidence process. A complete restoration will incorporate all three reverse-modelling processes. A detailed description of this methodology is given in Kusznir *et al*. (1995) and Roberts *et al*. (1998).

Figure 4c shows a restoration (to 160 Ma) of the Browse Basin section which has incorporated flexural unloading and decompaction during layer-by-layer backstripping, but has not incorporated reverse thermal-subsidence modelling. This leaves the water-loaded, post-break-up driving-subsidence within the restoration. If we look at the areas of the three presumed sea-level palaeobathymetric markers we see that (i) the Brecknock fault block lies below a residual bathymetry of ~1 km, (ii) the Scott Plateau lies below a residual bathymetry of ~3 km, and (iii) the Wilson Spur lies below a residual bathymetry of ~2 km. The residual bathymetry above these structures quantifies the water-loaded thermal driving-subsidence which has occurred since the Jurassic. It is clear that the driving subsidence is not uniform across the section and, therefore, the beta stretching-factors which have controlled the magnitude of thermal subsidence are also not uniform across the section.

Figure 4d shows a further restoration of the profile, with a profile of beta-factor below the restoration. This beta profile has been used to constrain reverse thermal-subsidence modelling of the post-break-up history, building a complete backstripped model in the process. In this revised model the three palaeobathymetric sea-level markers (at the Brecknock, Scott and Wilson areas) are restored back to, or close to sea-level, while the area inboard of Brecknock is restored to sea-level or a shallow-marine bathymetry. This restoration is, therefore, taken to be geologically acceptable and the geodynamic controls on this model may, therefore, be an acceptable description of some of the controls on the rift/break-up process.

The beta profile used to constrain the restoration in Figure 4d is very obviously non-uniform, showing considerable variation along the section in the value of beta-factor applied to define the thermal subsidence model. Four distinct areas can be recognized.

(1) Across the inboard SE part of the profile, from Brecknock landwards, the beta values applied range from 1.5 to 1.15. These are relatively low beta values, typical of an intra-continental rift basin rather than a continental margin. Applying beta values any higher than this across this area results in the shallow-marine Jurassic succession becoming emergent in the 160 Ma restoration, thus invalidating the restoration.
(2) Across the Scott Plateau, in the central part of the profile, the beta-factors applied jump to a uniform value of 5.0. This is a high beta-factor, typically indicative of highly attenuated continental crust close to a continental margin. This value of beta-factor restores the footwalls of the faulted volcanic topography on the Scott Plateau back to sea-level.
(3) On the Wilson Spur, towards the NW end of the profile, the beta-factor applied drops to 2.25. This still implies significant stretching/thinning in this area, but is obviously a lower value than that applied to the Scott Plateau. Applying this beta value at the Wilson Spur very nicely restores the erosional unconformity which caps the basalt SDRs back to sea-level at 160 Ma.
(4) At the NW end of the profile oceanic beta-factors have been applied, across the area of the profile thought to be Argo oceanic crust. This restores the bathymetry in this area to ~1 km, shallower than the typical depth of a mid-ocean ridge, implying that perhaps the oceanic crust is thicker than standard oceanic crust (typically 6.5–7 km) in this area. This would not be a surprise given the vigorous extrusive volcanism in the area, which classifies this margin as a ‘volcanic margin’.

Bringing these observations together, the inner Browse Basin has not developed in a straightforward manner from a Triassic/Jurassic rift basin into a highly extended continental margin. The high beta-factors applied across the Scott Plateau separate the inner basin from the Wilson Spur, which appears to be moderately stretched continental block located at the OCT. A possible implication of these observations is that the break-up to form the Argo oceanic margin originally attempted to occur at the site of the Scott Plateau, which if successful would have separated the Wilson Spur from the Browse Basin, on opposite sides of the spreading axis. For whatever reason, break-up at the Scott Plateau did not succeed and switched to the NW side of the Wilson Spur, leaving behind the highly attenuated Scott Plateau and the continental block of the Wilson Spur as part of the same margin.

Stretched continental blocks sitting outboard of failed break-up basins are not uncommon. Analogues in the north Atlantic constrained by high quality seismic refraction data would be the Faeroe Islands outboard of the Faeroes Shetland Basin and Hatton Bank outboard of the Rockall Trough (White & Smith 2009; Eccles *et al*. 2011).

Although not illustrated here, the backstripping exercise was repeated on two other regional lines across the Browse Basin

(AGSO 130–09 & 119–04 to the north and 128–02 & 119–02 to the south). Analysis of both lines, together with information from a seismic refraction line coincident with AGSO 119–06 & 128–01, confirmed the rapid transition from 'rift basin' of the inner Browse Basin to the highly attenuated continental margin of the volcanic Scott Plateau.

Additional support was also provided by 2D gravity-anomaly inversion along each of the three regional lines. When the gravity inversion was run applying the melt parameterization for a 'volcanic margin' (Fig. 1), the beta-factors predicted along the profiles were in good agreement with those predicted by post-break-up backstripping.

Norwegian Atlantic Margin

The Browse Basin example shows how we can use post-rift flexural backstripping to define a stretching model across a continental margin. Once a reliable stretching model is in place the backstripping can then be used to make predictions about palaeobathymetry and palaeostructure at all stratigraphic stages of the model (e.g. Kusznir *et al*. 2004, 2005). This was, indeed, done as part of the Browse Basin 2D case study, but the power of palaeobathymetric/palaeostructural prediction is best illustrated in 3D, when 3D data are available.

Figure 5 shows a summary of one model time-stage from the 3D study of the Norwegian Atlantic margin by Roberts *et al*. (2009). This figure illustrates the Møre & Vøring Basins backstripped to the Base Eocene, contemporary with margin break-up at this time. Figure 5a shows the map of break-up-related beta-factor which was used to drive the reverse thermal-subsidence modelling in 3D. The beta map itself was compiled from many different 2D backstripping models across the margin (including Roberts *et al*. 1997). The map of beta-factor not only defines the magnitude and distribution of lithosphere thinning associated with margin break-up; it is also a proxy for the break-up-related heat-flow anomaly experienced by the basins.

Figure 5b shows a 3D perspective view of the restored Møre & Vøring Basins at the Base Eocene. The upper surface of the model defines the predicted palaeobathymetry at this time; below that are the Paleocene and Cretaceous palaeostructural horizons for the Base Eocene model.

Figure 5c shows a map with more detail of the predicted Base Eocene palaeobathymetry. The map is calibrated by restoring the top of the Paleocene basalts of the outer Vøring Basin back to sea-level. The full significance of this map is described in Roberts *et al*. (2009). Finally, Figure 5d shows a map with detail of the Base Cretaceous subsurface palaeostructure at the Base Eocene. This horizon marks the top of the regional source rock in this area and so tracking its evolution through time defines the burial history of the source and provides information about palaeo-drainage routes and migration pathways within the basins.

Thus, we can see from the Browse Basin and Norwegian examples how post-rift/post-break-up flexural backstripping can enable us to define the stretching characteristics of the margin and then, using this information, make predictions about the palaeobathymetry and palaeostructure during the post-break-up evolution.

2D/3D SYN-KINEMATIC FLEXURAL BACKSTRIPPING

Post-break-up flexural backstripping is a straightforward technique to apply in situations where the base of the post-rift/post-break-up sequence can be readily defined. There are many continental margins, however, where this is not the case, particularly so in the case of margins where there are extensive mobile evaporites (salt), e.g. parts of the Brazilian and West African margins and the Gulf of Mexico. The presence of mobile salt makes the recognition of the base of the post-break-up sequence difficult on two counts: (i) the stratigraphic geometries and relationships of the post-break-up sequence are typically heavily modified both during and after their deposition by movement of the salt; (ii) the mobile salt itself preserves no original stratigraphic or structural relationships which might allow recognition of the syn-break-up/post-break-up distinction. Karner & Driscoll (1999*a*) and Karner *et al*. (2003) have argued, contrary to previous opinion, that the mobile Aptian salt of the Brazilian and West African margins is part of the syn-rift/syn-break-up sequence (and not post-break-up), in which case movement of the salt must, by definition, have deformed the base of the post-break-up section, making backstripping to a bathymetrically calibrated end-break-up restoration extremely impractical.

In addition to the complexities introduced by salt movement, the recognition of depth-dependent lithosphere stretching as common at rifted continental margins (Karner *et al*. 2003; Kusznir & Karner 2007) also makes identification of the base of the post-break-up sequence difficult in terms of applying traditional structural/stratigraphic criteria. Karner *et al*. (2003) and Kusznir & Karner (2007) have shown that it is possible for break-up-related thinning of the lithosphere to occur without the presence of extensive upper-crustal faulting. Thus, the syn-break-up sequence may be a thick unfaulted 'sag sequence' rather than a classic, faulted 'syn-rift' sequence. In such cases it is difficult to distinguish, using structural/stratigraphic relationships alone, the syn-break-up 'sag sequence' from the post-break-up 'sag sequence'.

In order to apply a backstripping methodology in areas where salt movement and/or depth-dependent stretching make reliable post-break-up backstripping difficult, we require a revised method which allows us to backstrip below the salt and into/below the syn-rift/syn-break-up sequence. In some cases backstripping to the top basement is the most appropriate target. We have developed such a technique, described here. The technique relies on a conversion of water-loaded subsidence estimates to estimates of stretching/thinning factor, without making an *a priori* assumption about whether the water-loaded subsidence is simply post-break-up in origin or whether it also incorporates a component of syn-break-up subsidence. This new form of subsidence analysis, incorporating both the syn-kinematic and post-kinematic sequences, will be described with reference to a case history from the Brazilian Campos Basin (e.g. Davison 1999; Karner & Driscoll 1999*a*; Mohriak *et al*. 2008), which lies to the north of the Santos Basin illustrated previously (Fig. 3).

Campos Basin, Brazil

Figure 6 shows the derivation of water-loaded subsidence for the base salt on a cross-section through the Campos Basin. The present-day section (Fig. 6a) is flexurally backstripped and decompacted without reverse thermal-subsidence modelling to the base of the salt (Fig. 6b). If the not-unreasonable assumption is made that the base of the salt (also the top of a fluvial lacustrine sequence, Mohriak *et al*. 2008) is a palaeobathymetric sea-level marker, then the residual bathymetry preserved in the backstripped restoration of Figure 6b is an estimate of the total water-loaded driving-subsidence to have affected the base salt horizon since its deposition in the Aptian. The water-loaded subsidence varies across the profile from ~0.5 km at the landward (western) end to ~5 km at the oceanic (eastern) end: a subsidence profile which is fully compatible with the location of the Campos Basin on the Atlantic continental margin.

By simply observing the subsidence profile we cannot discriminate whether the subsidence of the base salt is the product

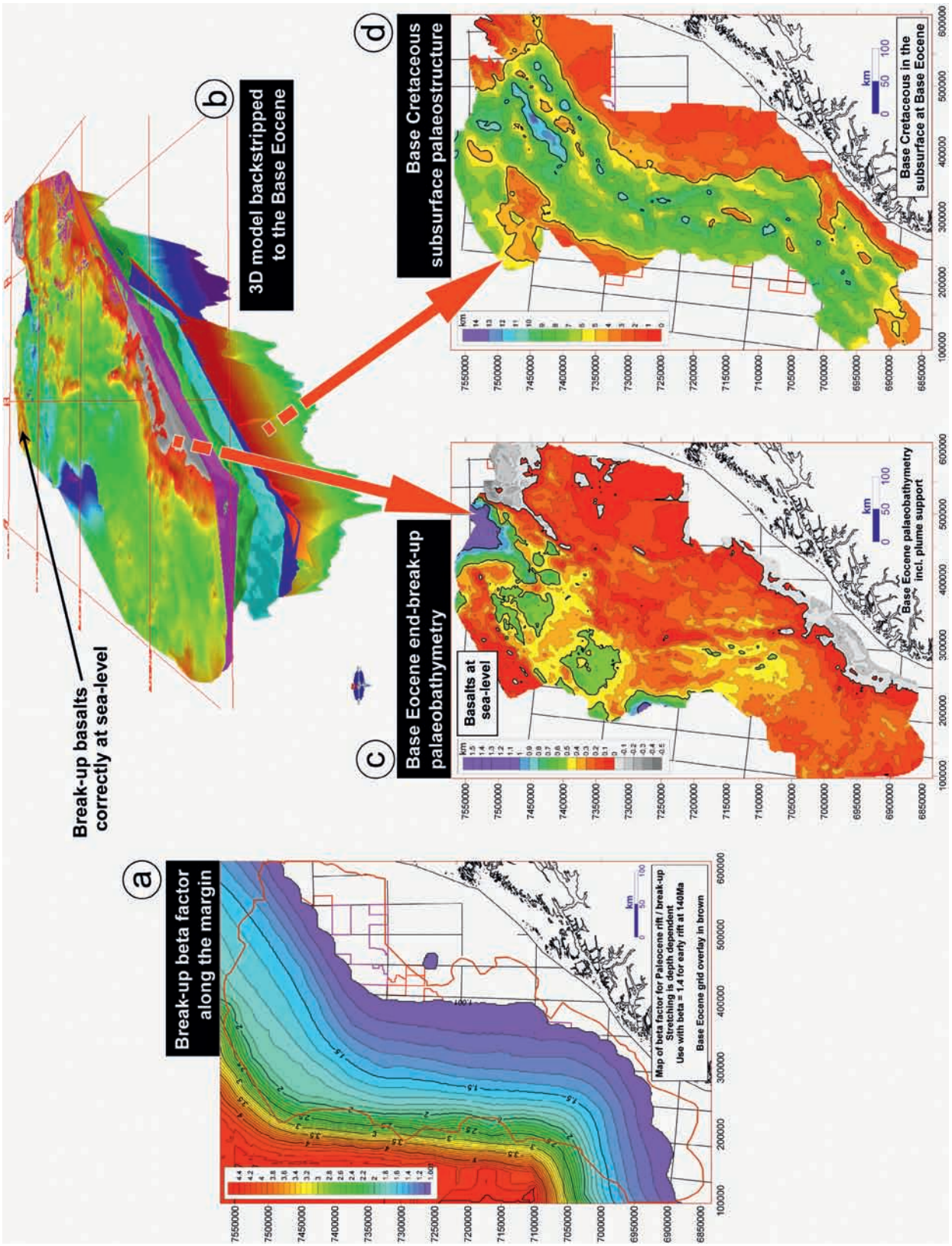

Fig. 5. 3D post-break-up flexural backstripping of the mid-Norway Atlantic margin (see Roberts *et al.* 2009 for full details). (**a**) Map of break-up-related beta-factor for the Norwegian margin, used to control reverse thermal-subsidence modelling in 3D. (**b**) 3D illustration of the flexurally backstripped model (Te 1.5 km) at the Base Eocene (break-up), reverse thermal subsidence modelling included in the backstripping. The upper surface of the 3D model (b) is the Base Eocene seabed geometry, shown in map form as predicted palaeobathymetry in (**c**). The deeper surfaces of the 3D model (b) are the Paleocene and Cretaceous horizons restored in the subsurface at the Base Eocene. The deepest of these, Base Cretaceous, is shown in map form as predicted subsurface palaeostructure in (**d**).

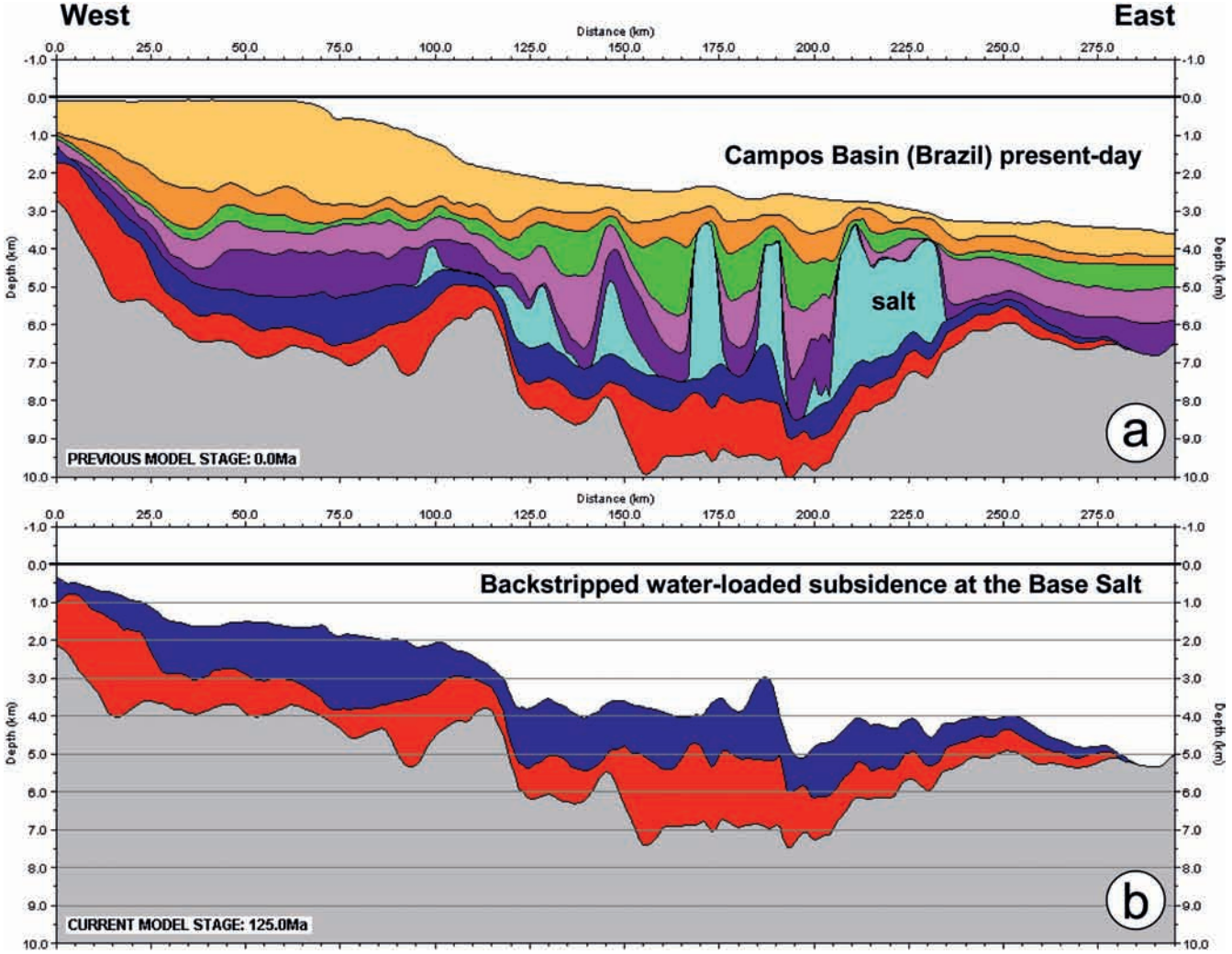

Fig. 6. (**a**) Present-day depth section across the Campos Basin Atlantic margin, offshore Brazil. Location in Figures 8–10 and as Line 1 in Figure 3. The key stratigraphic horizons are (i) highly mobile Aptian salt in light blue, (ii) the immobile Aptian Base Salt at the top of the underlying dark blue. Above the salt is a complete Aptian–present sequence, basement is grey. (**b**) Flexurally backstripped to the base salt (Te 3 km) with no reverse thermal-subsidence modelling applied. Residual bathymetry increases from ~0.5 km (NW) to ~5 km (SE) across the backstripped section as the OCT is approached. It is assumed that the base salt (top of a fluvial/lacustrine sequence) should, in fact, be restored to sea-level at this time and the residual bathymetry is, therefore, an estimate of the water-loaded driving-subsidence to have affected the section since the Aptian base salt.

of post-break-up thermal subsidence alone (St) or whether it results from a combination of syn-break-up subsidence (Si) plus subsequent post-break-up subsidence (St). Instead a quantitative means to make this discrimination and thus estimate stretching/thinning factors is required.

Converting water-loaded subsidence to thinning factor. The conversion of water-loaded subsidence to estimates of thinning factor is achieved using a modified version of the McKenzie (1978) subsidence model which makes allowance for volcanic addition as a result of decompression melting at high stretching factors (McKenzie & Bickle 1988; White & McKenzie 1989). The parameterization of melt addition with stretching is the same as that applied within the Greenhalgh & Kusznir (2007), Chappell & Kusznir (2008) and Alvey *et al*. (2008) gravity inversion scheme (Fig. 1b), thus there is an internal consistency between the input to and the output from both the gravity inversion and backstripping procedures.

Figure 7 shows three plots of the relationship (using the modified McKenzie model) between water-loaded subsidence and thinning factor ($1-1/\beta$) for an Aptian age rift/break-up event. Each plot illustrates how syn-rift subsidence (Si), post-rift subsidence (St) and the total subsidence (Si+St) evolve as thinning factor increases from 0 (no thinning) to 1 (complete crustal thinning, formation of oceanic crust). Thinning factor, rather than beta-factor, is used in these plots because the relationship between thinning and subsidence in the McKenzie model is approximately linear for both Si and St, whereas the relationship of subsidence to beta-factor is exponential. Common input parameters for each plot are a rift age of 125 Ma, an initial crustal thickness of 35 km and a crustal density of 2.80 g cm^{-3}. This combination of initial crustal thickness and density are thought to be suitably matched, but these parameters can be varied within the model. The magnitude of Si is dependent on the initial crustal thickness and the crustal density, but not the rift age. The magnitude of St is dependent on the rift age, but not crustal density and thickness. The magnitude of Si+St is, therefore, dependent on all three parameters.

The difference between the three plots in Figure 7 illustrates the sensitivity of subsidence to different parameterizations of volcanic addition during stretching. Figure 7a incorporates no volcanic addition and is, in essence, a straightforward plot of subsidence vs. thinning from the McKenzie

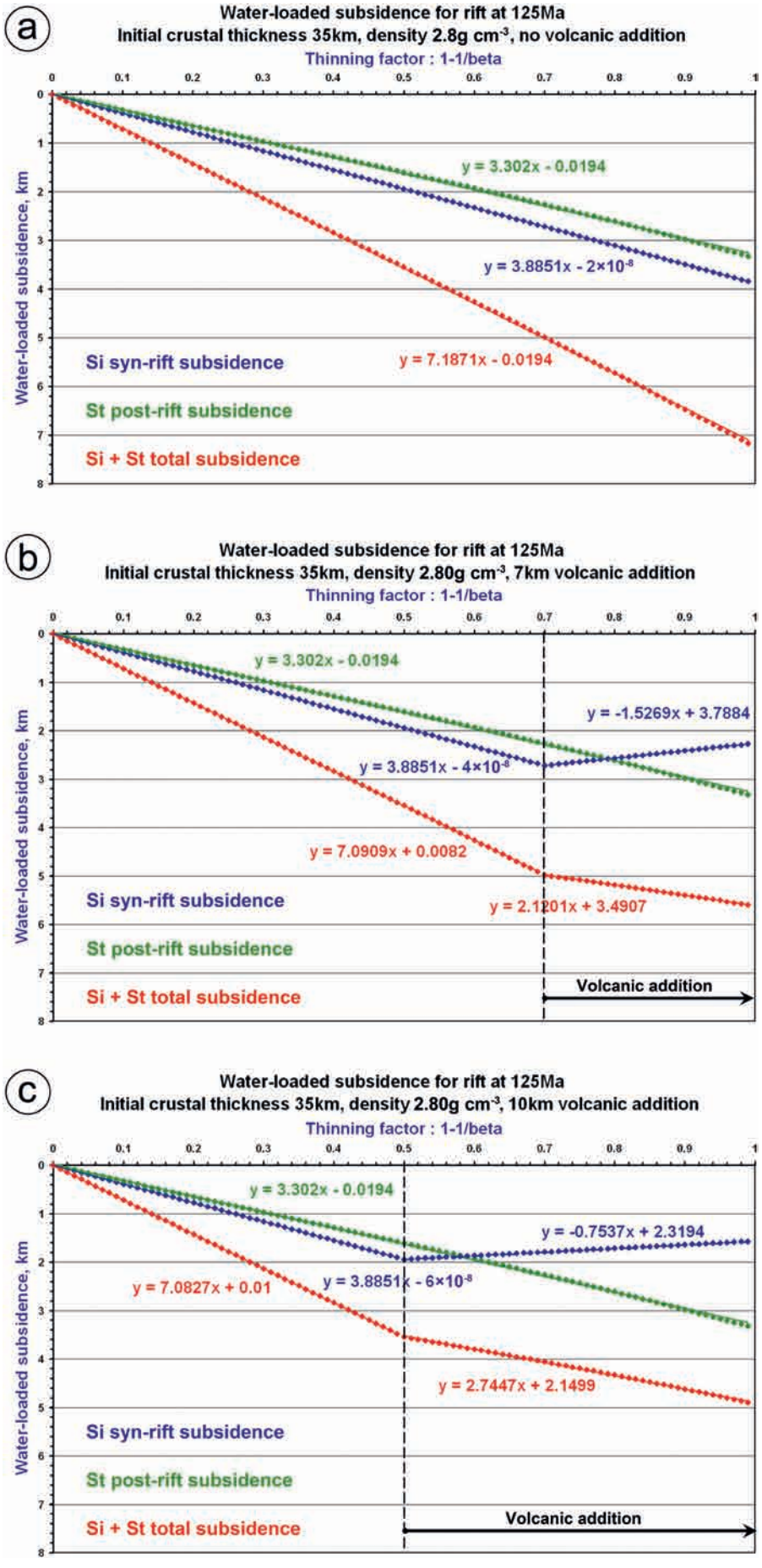

Fig. 7. Three plots showing how evolving water-loaded subsidence at a rifted margin, age 125 Ma (early Aptian), is related to thinning factor for three cases of volcanic addition. (**a**) No volcanic addition during stretching/break-up. (**b**) Up to 7 km of volcanic addition during stretching/break-up, beginning at a critical thinning factor of 0.7. This is the 'normal' rifted margin of Figure 1. (**c**) Up to 10 km of volcanic addition during stretching/break-up, beginning at a critical thinning factor of 0.5. This is the 'volcanic' rifted margin of Figure 1. The subsidence model follows McKenzie (1978), modified to incorporate the isostatic consequences of volcanic addition at high stretching. On each plot the instantaneous syn-rift/break-up subsidence (Si) is shown in blue, the time-dependent thermal subsidence (St) (125 Ma duration) is shown in green and the combined total subsidence (Si+St) of the basin/margin since rifting began is shown in red. The initial crustal thickness in each case was 35 km and the density of both initial crust and volcanic addition was 2.8 gm cm^{-3}; these two parameters affect the Si component but not St. Note how volcanic addition acts to buffer Si at high stretching and thus reduces the total Si+St at the present day. The straight line equations are used to convert backstripped maps/profiles of water-loaded subsidence to estimates of thinning factor (see Figs 6, 8–10).

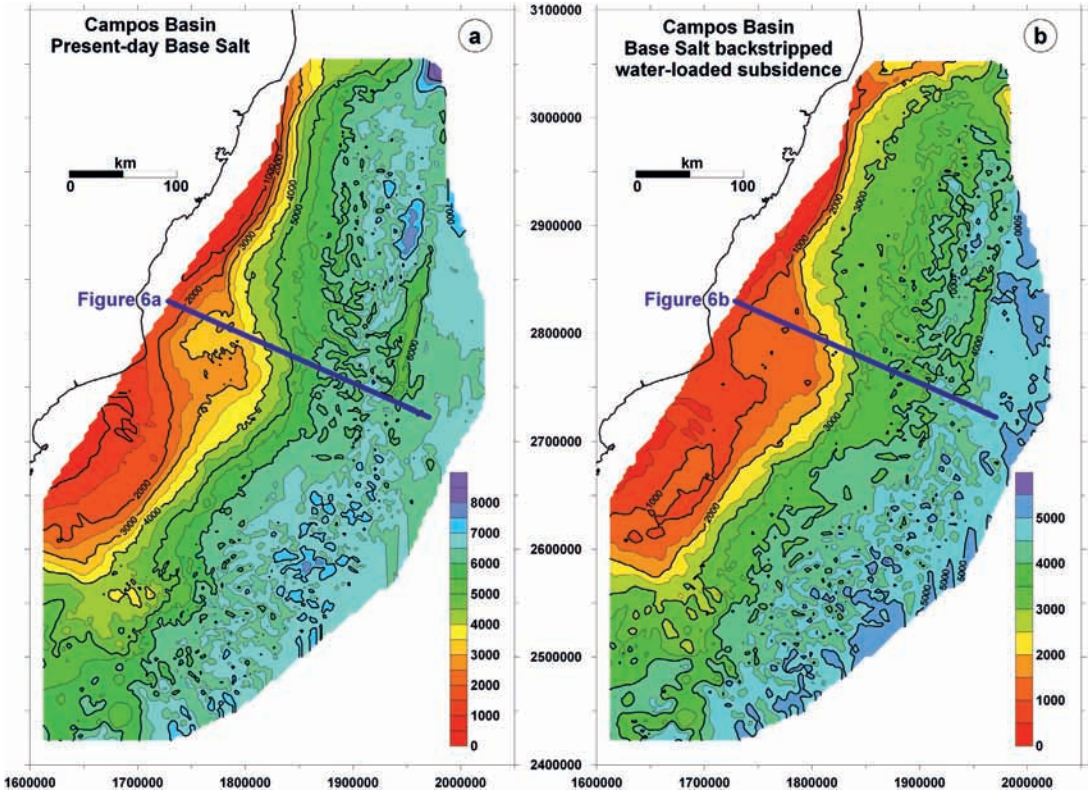

Fig. 8. (**a**) Map of present-day depth to base salt in the Campos Basin (Brazilian coastline to the west). The outer limit of the map lies within the zone of the OCT. (**b**) Flexurally backstripped in 3D to the base salt (Te 3 km) with no reverse thermal-subsidence modelling applied. Residual bathymetry increases from ~0.5 km (NW) to ~5 km (SE) across the backstripped map as the OCT is approached. It is assumed that the base salt (top of a fluvial/lacustrine sequence) should, in fact, be restored to sea-level at this time and the residual bathymetry is, therefore, an estimate in map form of the water-loaded driving-subsidence to have affected the Campos Basin since the Aptian base salt. This figure is directly comparable with Figure 6, which shows the same information in 2D cross-sectional form.

(1978) model, assuming a break-up age of 125 Ma. In this model Si has a maximum value of ~4 km at a thinning factor of 1.0. St has a corresponding maximum value of just above 3 km and the maximum total subsidence after 125 Ma is, therefore, slightly more than 7 km.

Figure 7b incorporates 7 km of volcanic addition during stretching, beginning at a critical thinning factor of 0.7 (Fig. 1). This is a melt parameterization thought to be characteristic of a 'normal' continental margin. In simple terms the process being described is a continued thinning of the pre-existing crustal basement through to a thinning factor of 1.0, but while this crustal thinning continues beyond a thinning factor of 0.7 new melt is added to the crust up to a maximum thickness of 7 km. This results in a buffering of Si, such that Si is actually reduced as the volcanic addition occurs. At a thinning factor of 1.0 the final value of Si is ~2.3 km (cf. ~4 km in Fig. 7a). This is the predicted magnitude of bathymetry above the newly formed 7 km-thick oceanic crust and is an acceptable bathymetry for a standard mid-ocean ridge.

Volcanic addition has no effect on the relationship between thermal subsidence and thinning factor, St being independent of crustal thickness. Thus, the St-vs.-thinning relationship in Figure 7b is the same as that in Figure 7a. The total subsidence (Si+St), however, is different between the plots, because of the Si contribution. Maximum total subsidence in Figure 7b is reduced to ~5.5 km, from ~7 km in Figure 7a.

Figure 7c shows the parameterization of volcanic addition for a 'volcanic margin'. Melt addition begins at a critical thinning factor of 0.5 and reaches a maximum thickness of 10 km. This buffers the maximum Si at thinning factor of 1.0 even further, to ~1.6 km, shallower than the bathymetry of a standard mid-ocean ridge. The St-vs.-thinning relationship once again remains unchanged, but the maximum total subsidence (Si+St) is reduced to ~5 km.

Within Figure 7 all of the illustrated relationships between thinning and subsidence are well described by a simple linear equation. This means that if we have an observation/calculation of water-loaded subsidence (e.g. Fig. 6b) there now exists a range of equations, covering a spread of geological assumptions, which can convert subsidence to estimated thinning factor.

3D syn-kinematic flexural backstripping. The 2D profile of water-loaded subsidence from the Campos Basin (Fig. 6b) can be converted to profiles of thinning factor by applying the relationships in Figure 7. The full power of this technique, however, is best illustrated in 3D and so the analysis will now move to a 3D map-based analysis. Figure 8 transcribes Figure 6 into 3D. Figure 8a shows a depth map of the present-day base salt in the Campos Basin. Figure 8b shows this horizon backstripped (without reverse thermal-subsidence modelling) to reveal total water-loaded subsidence of the base salt since the Aptian. This map can now be converted to estimates of thinning factor using the relationships in Figure 7.

At the outset we cannot tell simply by observing the subsidence captured in Figure 8b whether this subsidence is the product of Aptian–present post-break-up thermal subsidence alone (St only), or whether it captures both syn-break-up and post-break-up subsidence (Si+St) (Karner & Driscoll 1999*a*). The strategy towards such a discrimination is to apply a number of different subsidence conversions, producing a number of maps of the thinning factor, and

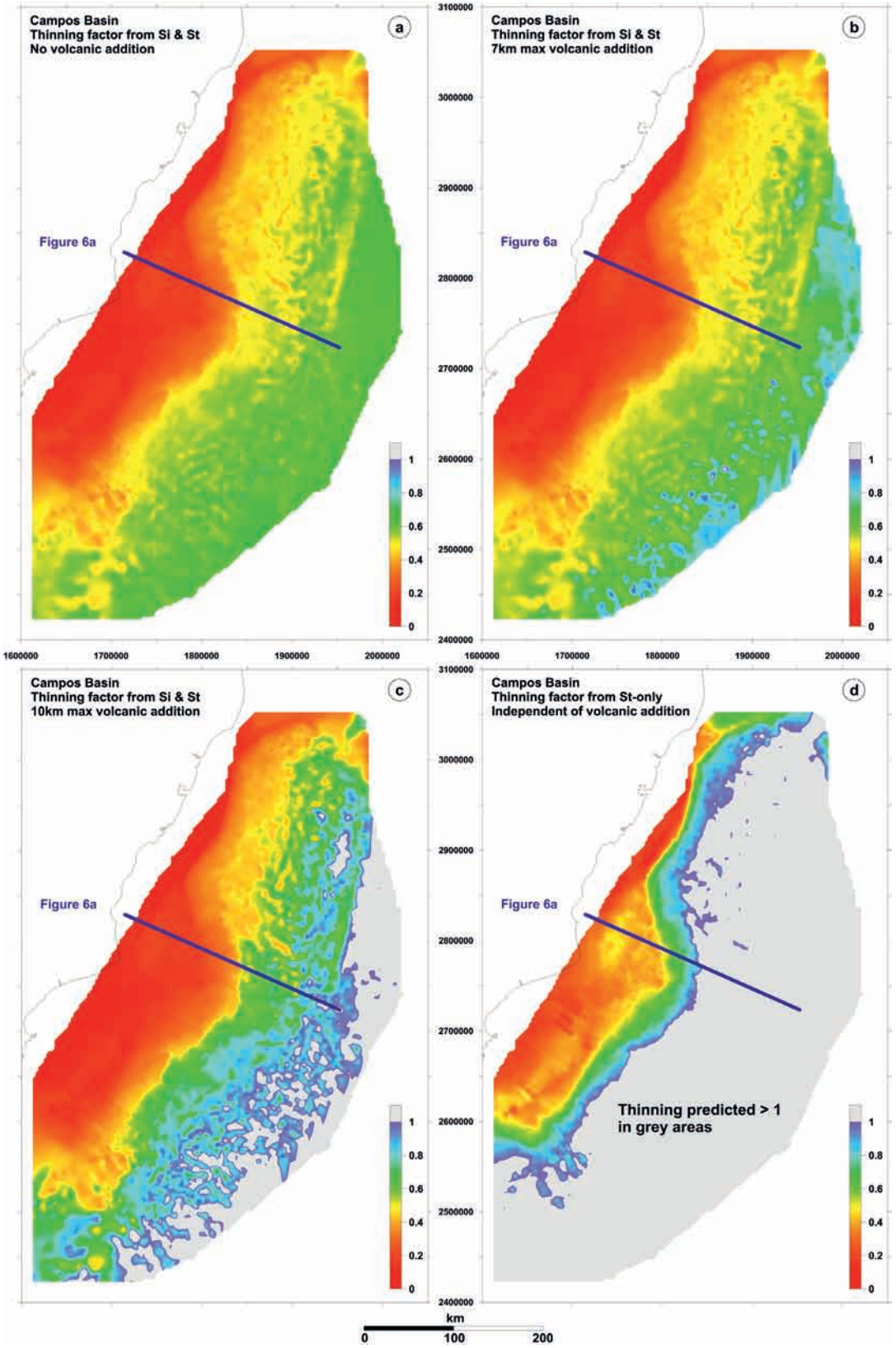

Fig. 9. Four maps of the thinning factor for the Campos Basin derived from the water-loaded subsidence map of Figure 8b, using the subsidence conversions of Figure 7. (**a**) Thinning factor assuming no volcanic addition, derived using the total subsidence (Si+St) relationship in Figure 7a. (**b**) Thinning factor assuming up to 7 km volcanic addition, derived using the total subsidence relationship (both linear segments) in Figure 7b. (**c**) Thinning factor assuming up to 10 km volcanic addition, derived using the total subsidence relationship (both linear segments) in Figure 7c. (**d**) Thinning factor assuming base salt subsidence has been St only, derived using the post-rift subsidence relationship which is the same in each plot of Figure 7. Note how, in the outer area of the basin, thinning factors increase from (a) to (d); (d) can be immediately discounted on the grounds of geological and geophysical implausibility (see text). Discussion in the text suggests that (b) may be the best-case model, although the sensitivities of (a) and (c) provide a useful range of uncertainty.

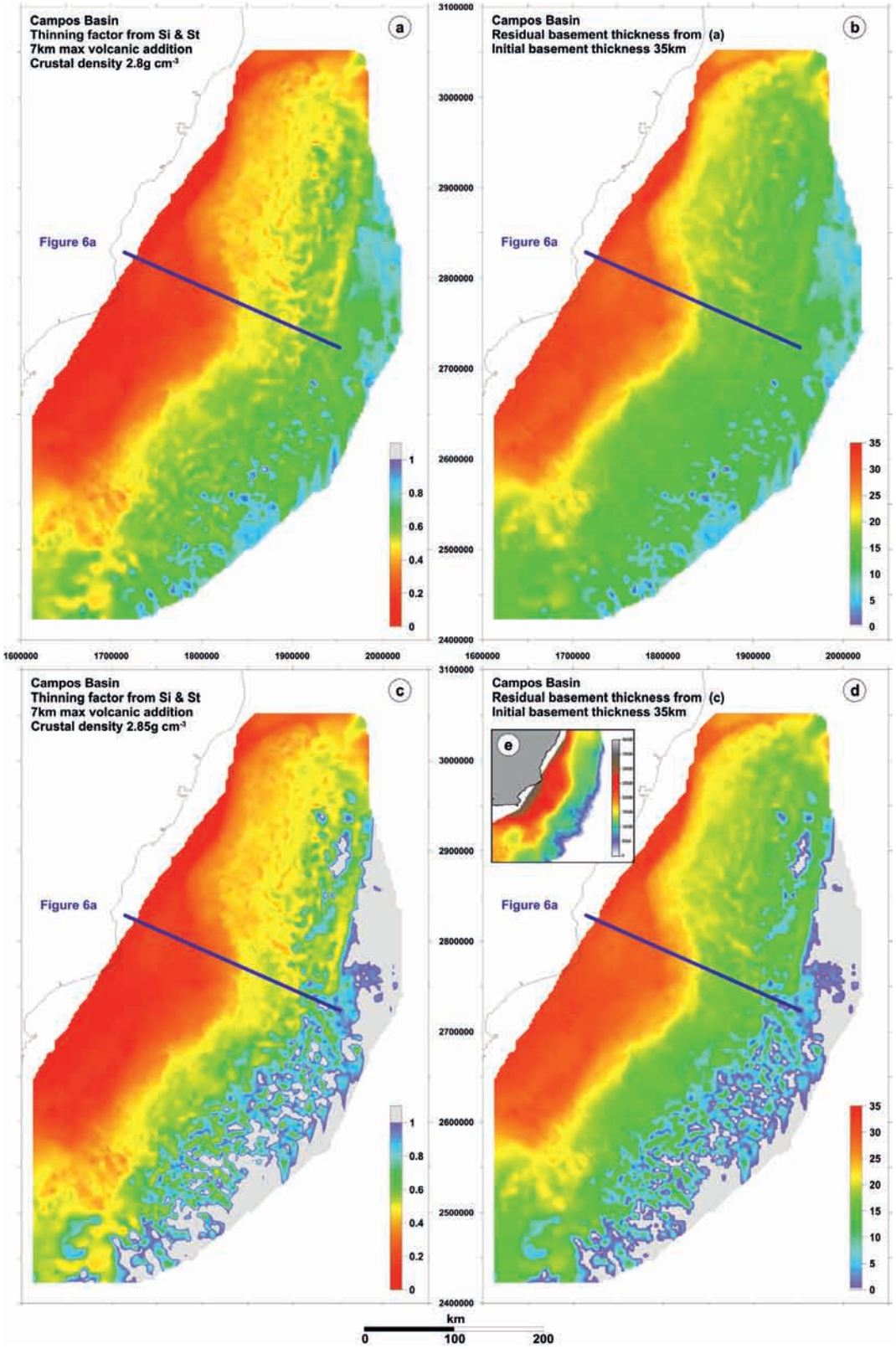

Fig. 10. Four maps, (**a**, **c**) showing thinning factor and (**b**, **d**) showing residual thickness of continental crustal-basement, derived from the water-loaded subsidence map of Figure 6b. (**a**) Thinning factor assuming up to 7 km of volcanic addition, derived using the total subsidence relationship (both linear segments) in Figure 7b. This map is the same as Figure 9b. (**b**) Residual crustal-basement thickness derived by applying (a) to an original crustal thickness of 35 km. (**c**) Thinning factor produced by changing the crustal and volcanic densities in Figure 7b to 2.85 g cm^{-3} (conversion not illustrated) and then using the revised total subsidence relationship (both linear segments). This predicts higher thinning factors as a result of raising the crustal densities. (**d**) Residual crustal-basement thickness derived by applying (c) to an original crustal thickness of 35 km. Note that oceanic crust (basement = 0 km) now encroaches on to the eastern edge of the map. (**e**) Inset map of residual crustal-basement thickness derived from gravity inversion using the same input parameters as (c) and (d). There is a clear correspondence between basement thickness estimated from 3D backstripping and from gravity inversion when the same basic parameters are used.

then see if there is an element of geological discrimination which can be applied to help focus on a best-case model.

Figure 9 shows four maps of the predicted thinning factor for the Campos Basin, derived from the water-loaded subsidence map of Figure 8b. On all four maps the graded-coloured area identifies the area in which the predicted thinning factor lies in the range 0 to 1. Any area coloured grey has a predicted thinning factor ≥1, from the application of the linear equation from Figure 7. A thinning factor of 1.0 defines complete attenuation by stretching and thinning of continental crust and lithosphere, and the formation of oceanic crust. A thinning factor >1.0 is not meaningful and, in fact, identifies subsidence which is not possible within the physical constraints of the McKenzie (1978) model. Figure 9a shows thinning factor predicted without the influence of volcanic addition (a rift basin or 'magma-poor' margin) and has been produced using the single linear equation for total subsidence (Si+St) in Figure 7a. Figure 9b shows thinning factor assuming that the Campos Basin is a 'normal' margin. The two linear equations (above and below the thinning factor of 0.7) for total subsidence (Si+St, Fig. 7b) have been used to produce this map. Figure 9c shows thinning factor assuming that the Campos Basin is a 'volcanic' margin, using the two linear equations for total (Si+St) subsidence in Figure 7c. Finally, Figure 9d shows thinning factor assuming that the subsidence is thermal subsidence only and has been produced using the common equation for thermal subsidence (St only) on all three plots in Figure 7.

Consider first Figure 9d, which assumes that subsidence of the base salt has been driven by thermal subsidence alone. This map presents two very serious problems to its acceptance, one geological and the other geodynamic. The geological problem is the predicted position of the COB, which by definition lies at a thinning factor of 1.0. Figure 9d shows the COB to lie quite close to the Brazilian coast, much closer than is normally considered likely. This prediction is contradicted by the presence of a thick pre-salt stratigraphic succession in the outer Campos Basin, east of the predicted ocean boundary. There should be no pre-salt stratigraphic succession if the base salt sits on oceanic crust. The geodynamic problem is the magnitude of the thinning factor predicted in the 'oceanic' area. In Figure 9d the grey area does not define a uniform oceanic thinning factor of 1.0; values of the predicted thinning factor rise to >1.5, indicating an impossible magnitude of thermal subsidence in the outer Campos Basin.

Taken together these two problems with the position of the predicted COB on Figure 9d suggest most strongly that the subsidence of the base salt in the Campos Basin cannot be explained as the product of thermal subsidence alone and an alternative explanation of the subsidence must be sought.

Figure 9a–c provides three possibilities. All show lower thinning factors than Figure 9d and the predicted oceanic area is either smaller or not present at all within the area of data coverage. In the inner Campos area (thinning factor <0.5) all three maps are identical, but they differ in the outer part of the basin where the magnitude of volcanic addition becomes relevant at higher stretching/thinning factors. In the outer margin area the model with no volcanic addition (Figs 7a & 9a) predicts the lowest thinning factors, the model with up to 7 km of volcanic addition (Figs 7b & 9b) predicts an intermediate range of thinning factors, and the model with up to 10 km of volcanic addition (Figs 7c & 9c) predicts the highest range of thinning factors and the largest area of potential oceanic crust (thinning factor 1) along the eastern margin of the data.

What is required next, in order to choose which of these three models is the best case, is an independent means of calibrating the amount of volcanic addition which occurred during continental break-up. This is provided by Mohriak *et al*. (2008, fig. 12) who show a depth profile across oceanic crust in the northern part of the Campos Basin (strictly the Espirito Santo Basin), within the area covered by our maps. The oceanic crust here has a uniform thickness of 7 km and suggests that the best-case model to use for volcanic addition, both during gravity inversion and subsidence conversion, will be that for a normal 'non-volcanic' margin, with 7 km of volcanic addition.

From the four solutions available in Figure 9 this allows us to choose Figure 9b as the best-case model for predicted thinning factor in the Campos Basin. This is a model in which thinning factors in the mapped outer margin area rise close to 1, but do not reach 1, predicting that the mapped area comprises highly thinned continental margin, with volcanic addition in the outer margin area, but is not fully formed oceanic crust. This might appear to be the definitive answer for the Campos Basin, but, as with most modelling of continental margins, there remains some underlying uncertainty.

Figure 10 shows a sensitivity test to the crustal density assumed in the subsidence conversions. Figure 10a reproduces the existing best-case map of thinning factor (Fig. 9b) and is complemented (Fig. 10b) by a map of residual continental-crustal basement thickness derived by applying the map of thinning factor to an initial crustal thickness of 35 km. Figure 10c shows a map of the predicted thinning factor which has been produced assuming all model parameters are the same as in Figure 10a, except for the crustal density, which has been raised to 2.85 g cm^{-3}. This is a crustal density at the upper end of the likely range for 35 km-thick initial crust. Figure 10d shows the complementary map of residual continental-crustal basement thickness. Comparison of Figure 10c with Figure 9c shows that the two maps show similar results at the outer margin, but are based on different input assumptions about crustal density and volcanic addition, illustrating a trade-off between the impact of the two parameters. Figure 10c shows that if the crustal density in the Campos Basin is closer to 2.85 g cm^{-3} than to 2.80 g cm^{-3} then the COB may actually lie within the mapped area and not immediately to the east.

The bulk density of the crustal basement below the Campos Basin cannot be measured directly. Figure 10a/b & c/d should, therefore, be taken as bracketing the likely range of admissible outcomes, although the seismic profiles of Mohriak *et al*. (2008, figs 11–13), published after our own analysis was completed, suggest that Figure 10c/d, with oceanic crust lying within the mapped area, may be the best solution against available geological calibration.

Comparison with results of gravity inversion. In parallel with the subsidence modelling of the Campos Basin a full gravity inversion was performed, using the same set of stratigraphic grids to constrain sediment thickness. Figure 10e shows the map of predicted residual crustal basement thickness which results from an inversion using crustal density 2.85 g cm^{-3}, reference Moho depth and initial crustal thickness 35 km and 7 km maximum volcanic addition, i.e. the input parameters match those of Figure 10c/d.

The maps of predicted basement thickness from the gravity inversion and the 3D subsidence analysis are comfortingly similar. This does not mean that the maps are correct, but it shows that by tackling the same problem in more than one way we can produce a consistent set of answers using the same fundamental geological controls on the models. Confidence in the answers is, therefore, increased.

QUANTIFYING UPPER-CRUSTAL FAULT EXTENSION

Estimating the seismically observed extension on upper-crustal faults by applying quantitative forward models of rift-basin

formation is a well-established method (e.g. Marsden *et al*. 1990; Kusznir *et al*. 1991, 1995, 2004, 2005; Roberts *et al*. 1993, 1997; Magnavita *et al*. 1994; Driscoll & Karner 1998; Karner & Driscoll 1999*a*, *b*; Karner *et al*. 2003; Davis & Kusznir 2004; Kusznir & Karner 2007). These studies began by looking at intra-continental rift basins and then moved to the deep-water geology of rifted margins.

During the course of these studies an important distinction was eventually made between the extension observed in rift basins and the extension observed at continental margins. Within rift basins the magnitude of extension observed on upper-crustal faults was found to be balanced by estimates of whole-crust or whole-lithosphere extension made by other observational/modelling techniques. At rifted margins, however, the amount of extension observed on upper-crustal faults was in each case found to be less than the extension predicted to have affected the whole crust or whole lithosphere, as summarized in Davis & Kusznir (2004) and Kusznir & Karner (2007). This has led to the suggestion that depth-dependent stretching of the lithosphere, first hypothesized by Royden & Keen (1980), may be an inevitable consequence of the process of continental break-up (e.g. Kusznir & Karner 2007; Huismans & Beaumont 2008, 2011).

The example presented here returns to the Browse Basin of NW Australia, discussed previously (Fig. 4). Figure 11a shows the outer part of the Browse Basin seismic line AGSO 119–06 & 128–01, from the Brecknock structure NW to the ocean. Figure 11b shows a whole-crustal syn-rift forward model of this section, produced using the flexural-cantilever model of continental lithosphere extension (e.g. Kusznir *et al*. 1991). The model is constrained by the extension measured on the observed faults which affect the Wilson Spur, Scott Plateau and the Brecknock structure at the level of the top of the Jurassic volcanics. When setting up the model, individual faults have each been given the maximum extension which the seismic interpretation will allow. The model produces quite an accurate geometrical structural template of the faulting as observed on the seismic line, although we readily acknowledge that the basalt layer itself may mask seismic imaging of any deeper fault structure below the volcanics.

Figure 11c shows the thinning-factor profile ($1-1/\beta$) of lower-crustal (and mantle) ductile stretching associated with this model (Stretch model 1); the brittle extension on the faults is balanced through the deeper part of the model by the ductile stretching captured in the thinning profile. The maximum value reached by the thinning-factor profile is ~0.3 (β=1.45, or 45% extension). Figure 11c also shows the matching part of the best-case thinning-factor profile from flexural-backstripping subsidence analysis (β-profile in Fig. 4d), in which the predicted thinning factor across the Scott Plateau is 0.8 (β=5.0 or 500% extension). There is, therefore, an extension discrepancy of an order of magnitude between the seismically imaged fault extension and the lithosphere thinning predicted by backstripping. It is difficult to argue that an extension discrepancy of this magnitude can be attributed to unimaged faulting (Reston 2007) and instead the extension discrepancy would appear to be indicative of depth-dependent stretching during break-up of the Browse Basin margin. This should perhaps not be too surprising, as the continental margin of the Exmouth Plateau, to the south of the Browse Basin on the west Australian shelf, is one of the 'type areas' for the recognition of depth-dependent-stretching (Driscoll & Karner 1998; Karner & Driscoll 1999*b*; Kusznir & Karner 2007).

Figure 11d shows an alternative fault-controlled model for the outer Browse Basin, in which the structure is dominated by two high-extension, highly rotated normal faults which have exhumed a large area of fault plane resulting in 'core-complex' or 'detachment' geometries (cf. Kusznir *et al*. 1995, fig. 18). Figure 11c shows the thinning-factor profile of ductile stretching associated with this model (Stretch model 2), which provides a good match with the thinning-factor profile from flexural-backstripping subsidence analysis. This illustrates what the structure of the upper crust in the outer Browse Basin would need to look like in order for the fault-controlled extension to balance the whole-lithosphere thinning predicted by backstripping. It is not impossible that Figure 11d provides a template for the fault-controlled structure of the outer Browse Basin, with the highly rotated faults obscured by the basalt layer, but, given the currently available seismic data (Figs 4a & 11a), the more conservative fault model of Figure 11b is preferred, together with the implication for depth-dependent lithosphere stretching at the margin.

The corresponding crustal cross-section from gravity inversion is shown in Figure 11e. The thinning-factor profile produced from this gravity inversion is also shown in Figure 11c and shows good agreement with that predicted by the flexural-backstripping subsidence analysis.

FORWARD MODELLING THE KINEMATICS OF BREAK-UP

The techniques described so far, which comprise the majority of the workflow, all allow evaluation of margin geometry and the continent–ocean relationship within the context of observations and data from present-day margins. We believe that this initial stage of analysis, in which we attempt to understand and characterize margin geometries in their present-day setting, is the crucial first step that must be undertaken before any further, and perhaps more complex, modelling is performed or before any further inferences are drawn about the processes associated with margin evolution and continental break-up.

Once the present-day margin geometry is understood, at least in terms of its first-order characteristics, then we can begin to investigate the progressive development of a margin, from rift to break-up, using observations and conclusions from analyses already in place as constraints. This is illustrated in Figure 12, where our existing understanding of the Browse Basin (Figs 4 & 11) is taken a step further with a conceptual forward model illustrating the rift to break-up process.

Kusznir *et al*. (2005) and Kusznir & Karner (2007) have described a new model for rifted margin break-up which views the progressive evolution of a margin as the initiation of the sea-floor spreading process rather than the culmination of the intra-continental rifting process. It does this by modelling the thinning of continental lithosphere leading to break-up and sea-floor-spreading initiation as being generated not just by pure-shear stretching and passive upwelling driven by far-field plate-boundary forces, but also by to additional upwelling assisted by thermal and melt buoyancy.

Previous illustrations of break-up incorporating upwelling-divergent flow (Kusznir *et al*. 2005; Kusznir & Karner 2007) have shown models which are either single-sided (one margin) or double-sided (conjugate) but symmetrical. The model illustrated here (Fig. 12) is conjugate and asymmetrical, illustrating how geometrically distinct margin pairs may result from the progressive break-up process. The model is at the scale of the whole lithosphere and, therefore, at the scale reproduced here, it contains a necessary simplification of detailed structural geometries which can be resolved at the seismic scale.

The modelled break-up process begins (Fig. 12a) with a pure-shear rift basin driven by far-field plate forces. In many cases, perhaps the majority, this rift basin will not evolve to a paired continental margin. Braun *et al*. (2000) and Nielsen & Hopper (2004) have shown that thermal and melt buoyancy is important at slow-spreading ocean ridges, particularly if wet

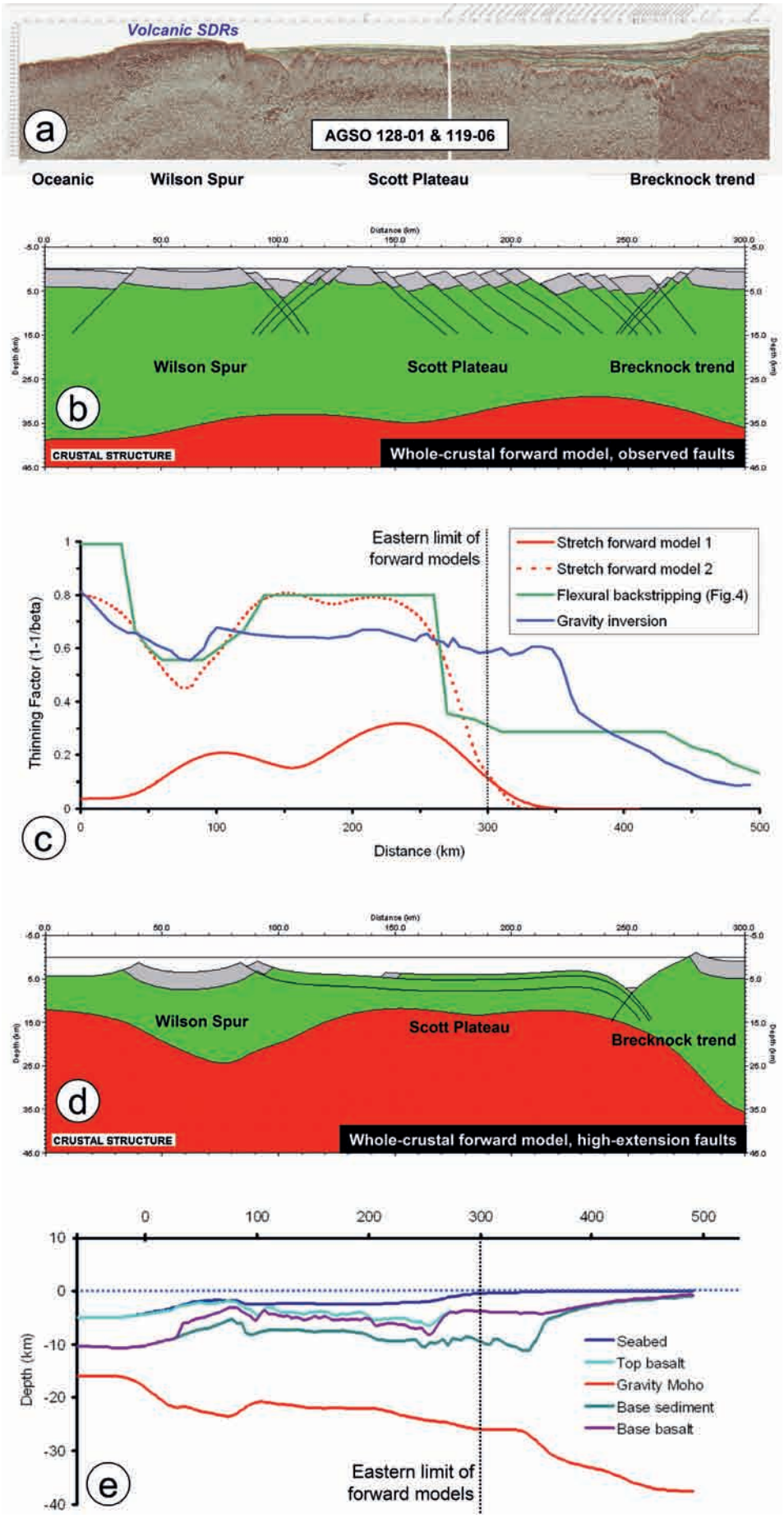

Fig. 11. Upper-crustal extension, Browse Basin continental margin, NW Australia. (**a**) Composite regional seismic depth profile extending from the Brecknock structure in the SE to the edge of the Argo oceanic abyssal plain in the NW. This is the outer part of Figure 4a, located in Figure 4e. © Commonwealth of Australia (Geoscience Australia) 2011. (**b**) Whole-crustal flexural-cantilever forward model (Stretch 1) of the fault-structure imaged in (a) (formation of oceanic crust west of Wilson Spur not included). The thinning-factor profile associated with this model is shown in (c). Maximum fault-controlled thinning factor is ~0.3 (β=1.45). (**c**) Comparison of thinning-factor profiles determined by flexural cantilever forward models (Stretch 1 and 2) shown in (b) and (d), thinning factor determined from flexural-backstripping subsidence analysis (Fig. 4d) and gravity inversion shown in (e). A maximum thinning factor of 0.8 (β=5) is required for the Scott Plateau from subsidence analysis, implying that lithosphere thinning was here approximately an order of magnitude greater than fault-controlled stretching. (**d**) Alternative fault model (Stretch 2) for the outer Browse Basin, in which fault-controlled stretching matches the implied whole-lithosphere thinning of ~0.8 from subsidence analysis (c). In this model the deep structure of the Scott Plateau is dominated by exhumed and highly rotated fault-plane rather than the observed tilted fault-blocks. The model in (d) cannot be ruled out, but we prefer the more conservative model in (b) (see text). (**e**) Corresponding crustal cross-section, showing Moho depth, determined from gravity inversion, thinning factor profile in (c).

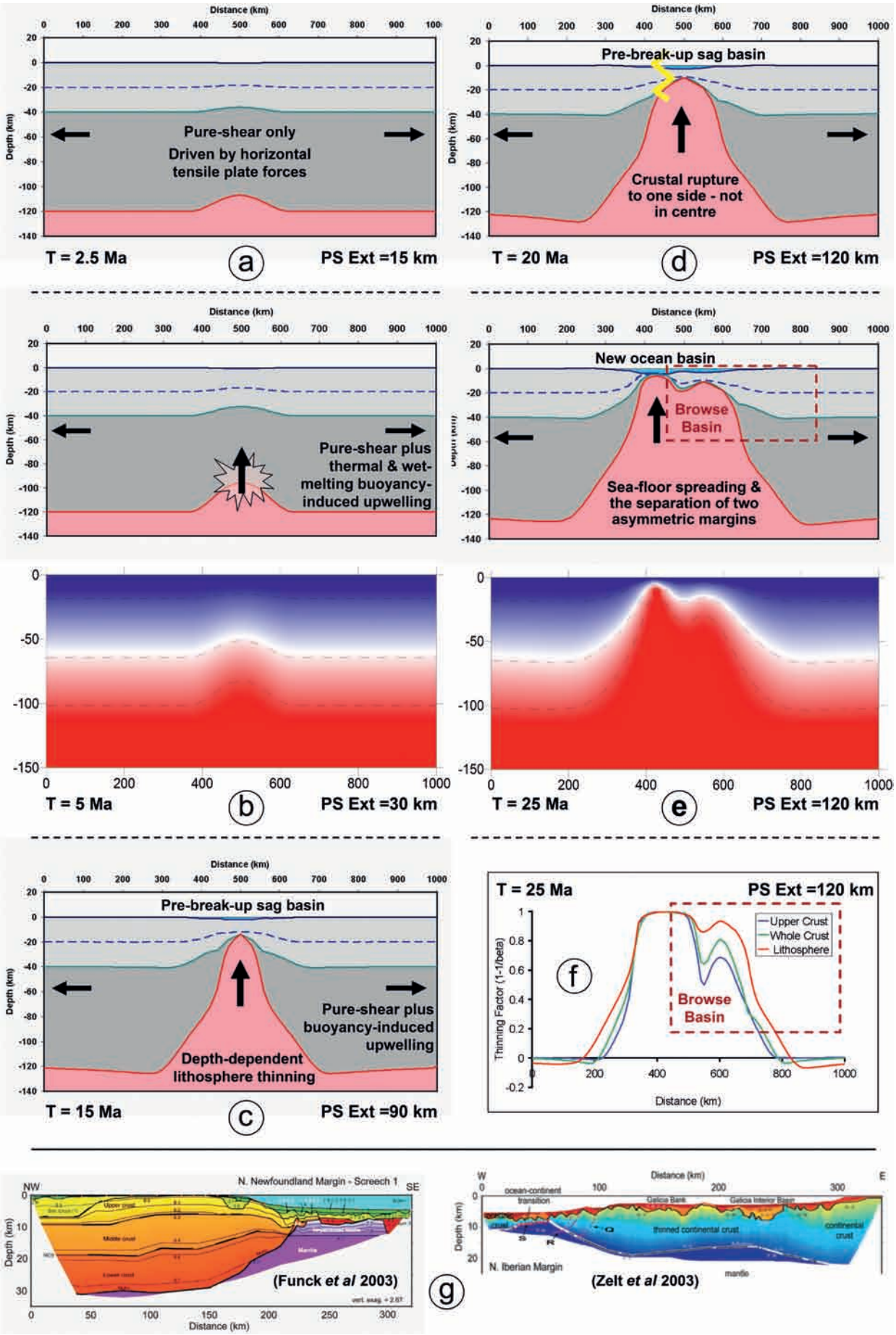

melting occurs. Fletcher (2009) has hypothesized that a similar process of thermal and melt buoyancy at the base of the continental lithosphere could be the trigger mechanism by which a rift basin evolves into a rifted margin at which the lithosphere-thinning deformation process is assisted by buoyancy-driven upwelling (a form of small-scale convection) in addition to pure-shear extension.

Figure 12b illustrates the inception of buoyancy-assisted upwelling below the rift. This provides an additional thinning of the middle and lower continental lithosphere as the rifting lithosphere continues to extend by pure-shear extension (Fig. 12c). With time the buoyancy-assisted upwelling penetrates to a shallower level in the lithosphere, contributing to the thinning of the continental lithospheric mantle and the lower continental crust. The relatively cooler, brittle, seismogenic upper continental-crust is, however, assumed to stretch and thin only by pure shear, analogous to the oceanic lithosphere deformation processes thought to occur at slow-spreading ocean ridges (Cannat 1996).

A natural consequence of continental lithosphere deformation by pure shear accompanied by buoyancy-assisted upwelling is depth-dependent stretching/thinning in which, as the flow field propagates upwards from depth, the mantle and lower crust are thinned more than the upper crust (Fig. 12c). This may produce a pre-break-up sag basin, superimposed on the original rift basin, in which the measured subsidence presumed to result from total crustal thinning is greater than can be accounted for by the extension observed on upper-crustal faulting. Kusznir & Karner (2007, fig. 6) have identified the sub-salt basin offshore Angola as a possible pre-break-up sag basin, situated on a margin which eventually evolved to full break-up.

It is also possible, however, that pre-break-up sag basins can be preserved without evolving to continental break-up. Examples of such basins may be the Nam Con Son Basin (Roberts *et al*. 1999) and the Faeroes Shetland Basin (Fletcher 2009; Fletcher *et al*. in press), both of which are broadly symmetrical intra-continental basins in which anomalously deep subsidence is observed by comparison with the measured magnitude of extension by upper-crustal faulting.

The upper part of the continental crust (and lithosphere) is cold and brittle and, for this reason, the buoyancy-induced upwelling cannot propagate to the Earth's surface. The transition from pre-break-up sag basin (Fig. 12c) to seafloor spreading must, therefore, ultimately result from extreme upper-crustal thinning by brittle extension, superimposed on an already-thinned crustal template (e.g. Manatschal *et al*. 2007). Once rupture of the continental lithosphere has occurred and seafloor spreading has commenced, lithosphere and asthenosphere deformation is modelled as upwelling-divergent flow (Spiegelman & Reynolds 1999).

If the final brittle failure occurs above the axis of the upwelling divergent flow field then a broadly symmetrical margin pair will result (see models of Kusznir & Karner 2007). If, however, final brittle failure occurs off-axis to the flow field and, therefore, towards one side of the pre-existing basin (Fig. 12d), an asymmetrical margin pair will result (Fig. 12e) and the new focus of seafloor spreading will migrate (effectively a 'ridge jump') to lie between the newly formed margins.

At such an asymmetrical margin pair one margin will be narrow and sharp, with little transition between thick continental crust and oceanic crust. The other margin will be wide and diffuse, with a large area of thinned continental crust lying between the ocean and the continental hinterland (Fig. 12e). Both margins will be affected by depth-dependent lithosphere stretching/thinning resulting from the break-up process, but the distribution of thinning will be very different on the two margins (Fig. 12f).

The wide, diffuse (right) margin of Figure 12e provides a good conceptual analogue for our understanding of the crustal structure of the Browse Basin (Figs 4 & 11). The marked variations in crustal thickness predicted by backstripping and gravity inversion across the Inner Browse Basin, the Scott Plateau and the Wilson Spur (Figs 4 & 11) are readily apparent. In addition, our prediction that lithosphere stretching/thinning across the outer Browse Basin (in particular across the Scott Plateau) was markedly depth-dependent, with whole-lithosphere thinning greater than upper-crustal thinning, is captured by the forward model (Fig. 12f). In this instance we have not illustrated a direct calibration of the forward model to data from the Browse Basin, but, within the forward modelling workflow, calibration of model predictions against (a) present-day bathymetry, (b) backstripped water-loaded subsidence and (c) free-air gravity anomaly are all possible (e.g. Kusznir & Karner 2007). The model incorporates a full lithosphere temperature history (Figs 12b, e) and, therefore, top basement heat flow and subsidence history can be predicted at any point across the conjugate margin pair.

The conjugate margin to the Browse Basin has now been lost by collisional accretion to SE Asia and so we do not know its break-up geometry. A well-documented example of a fully preserved asymmetrical margin pair is the Newfoundland–Iberia Atlantic conjugate (Hopper *et al*. 2007; Manatschal *et al*. 2007; Tucholke *et al*. 2007). Figure 12g shows the crustal profiles of Funck *et al*. (2003, Newfoundland) and Zelt *et al*. (2003, Iberia), in which Newfoundland is seen to be a narrow, sharp margin and Iberia is a broad margin with a wide region of highly thinned continental crust (cf. the Browse Basin). Kusznir & Karner (2007) have previously modelled and calibrated each of these margins individually, but by placing them in their conjugate context the crustal-scale similarities to the geometry of the model conjugate pair (Figs 12e, f) are illustrated. The forward model provides an explanation for the asymmetry of the Newfoundland-Iberia conjugate pair as a direct consequence of the rift to break-up process.

Fig. 12. Progressive forward model of the break-up process at an asymmetrical continental-margin pair, built upon earlier kinematic models of Kusznir *et al*. (2005) and Kusznir & Karner (2007). (**a**) Lithosphere structure (crust light grey, mantle-lithosphere dark grey, asthenosphere pink) after an initial rift accommodating 15 km pure-shear extension. Initial lithosphere thickness 120 km. (**b**) Lithosphere structure after 30 km pure-shear extension and the inception of buoyancy-induced upwelling (upper panel), with a cross-section of the lithosphere thermal structure at this time shown below (blue, Earth's surface = 0°C; red, base lithosphere into asthenosphere = 1300°C). (**c**) Lithosphere thinning by buoyancy-assisted upwelling (plus continued pure-shear) results in depth-dependent thinning and the formation of a pre-break-up sag basin in which subsidence is greater than can be accounted for by upper-crustal faulting. (**d**) Final crustal rupture by brittle extension occurs to one side of the pre-break-up basin. (**e**) A new ocean basin forms, separating an asymmetrical conjugate margin pair; the asymmetry results entirely from the kinematics of the break-up process (upper panel), with a cross-section of the lithosphere thermal structure at this time shown below (blue, Earth's surface = 0°C; red, base lithosphere into asthenosphere = 1300°C). The wider (right) margin is an analogue for the Browse Basin (Figs 4 & 11). (**f**) Thinning factor for model stage (e) at three levels within the lithosphere (upper crust, whole crust, whole lithosphere). The thinning-factor curves do not overlie each other on either margin, indicating depth-dependent stretching/thinning during the break-up process. The curves on the right margin are an analogue for the Browse Basin. (**g**) Crustal cross-sections for Newfoundland (Funck *et al*. 2003) and Iberia (Zelt *et al*. 2003), which provide an analogue for the full asymmetrical margin conjugate pair of (e).

DISCUSSION

What we have attempted to show is that while no one single analytical or modelling technique can provide complete insight into the geodynamic history of rifted margins, the application of a number of complementary techniques will take us further in our understanding than simply working with one technique alone. The case studies used here to document the workflow have been taken from a number of different margins in order to illustrate a diversity of approach. When applied to a single margin, however, the varied techniques combine with great effect, providing results which are scientifically relevant and which feed into the exploration process. It is important to point out that the workflow is not static and continues to evolve with each case studied and will hopefully continue to do so as the techniques themselves improve and as data from more margins become available.

Currently the workflow comprises application of:

- 2D/3D gravity inversion, with embedded thermal correction and incorporation of volcanic addition;
- 2D/3D post-break-up flexural backstripping;
- 2D/3D syn-kinematic flexural backstripping, with prediction of volcanic addition;
- quantifying upper-crustal extension, with comparison to other measurements of crust/lithosphere thinning;
- forward modelling the kinematic history of break-up for a conjugate margin pair.

In combination these techniques provide information about a number of aspects of rifted margin geodynamics, which then feed information into the exploration process.

- *Present-day crustal thickness and depth to Moho*. Mapped variations in crustal thickness reveal crustal structure in 3D from the continental hinterland out into the ocean basin. When exploring a new margin understanding the distribution of crustal thickness is of critical importance because it is the crustal basement thickness which controls the radiogenic heat flow from the basement into the overlying sediments.
- *The possible presence or absence of volcanic addition to the crust during break-up*. The amount of volcanic addition impacts upon the predicted distribution and thickness of the remaining thinned continental-crustal basement. Where volcanic addition has occurred, total present-day crustal thickness (predicted by gravity inversion or backstripping to estimate the thinning factor) will comprise a combination of attenuated crustal basement plus new volcanic addition. If the amount of volcanic addition can be estimated then so too can the residual thickness of the radiogenic crustal basement (Cowie & Kusznir 2012). Where volcanic addition is predicted to have completely replaced crustal basement (thinning factor of 1) this provides an indication of the likely presence of oceanic crust rather than highly extended continental margin. Oceanic crust makes no radiogenic contribution to heat flow into the overlying sediments and will also typically be indicative of a sustained deep-water depositional environment. Knowing where oceanic crust may be present is, therefore, an exploration requirement.
- *The distribution of the stretching/thinning factor across the margin*. Not only does constraining the stretching/thinning factor allow calibration of crustal thickness, it also allows calibration of the mantle-derived component of the rift/break-up heat flow anomaly (McKenzie 1978). Unlike the radiogenic heat flow contribution from within the crustal basement, this is not constant through time after break-up, but rather decays exponentially. It is the combination of background radiogenic heat flow plus the transient break-up-related thermal anomaly which provide an estimate of total heat flow into the overlying sediments.
- *Stretching mechanisms during margin break-up*. Depth-dependent lithosphere stretching/thinning is now widely recognized as a likely process at rifted continental margins (Davis & Kusznir 2004; Kusznir & Karner 2007). The operation (or not) of depth-dependent stretching can be recognized by estimating and comparing extension/thinning at different levels of the crust and lithosphere. Understanding how and why depth-dependent stretching operates is of fundamental importance to understanding the progressive break-up of a margin, but it is also important within the exploration context. The main radiogenic contribution to top-basement heat flow is thought to come from upper-crustal basement rather than the lower crust. If the lower crust and mantle are preferentially thinned by comparison with the upper crust then upper-crustal radiogenic heat productivity may still be preserved, providing higher heat-flow estimates than would be made from the application of a depth-uniform lithosphere-thinning model (Kusznir *et al*. 2005).
- *Palaeobathymetric history*. By using 3D-flexural backstripping we can produce models of the full post-break-up palaeobathymetric history of a margin (e.g. Roberts *et al*. 2009). This, in turn, has clear input into modelling depositional environments and source/reservoir distribution on the margin. If we extend the backstripping into the syn-break-up interval then we can provide estimates of how much rapidly developed accommodation space became available early in the margin's history as a consequence of the break-up process itself and prior to post-break-up thermal subsidence.
- *Palaeostructural history*. Palaeobathymetric maps provide information about the evolving surface structure of a basin or margin, but below the palaeo-seabed subsurface-horizon maps provide a full 3D structural model for the subsidence history of the margin. This can be particularly important for looking at how the subsidence process and associated sediment loading has affected structural gradients for fluid migration within the subsurface.

These examples provide insight into how integrated geodynamic modelling can provide input to many levels of the exploration process. They show how ongoing scientific investigations into margin structure and margin evolution feed directly back to help in the commercial assessment of a margin's hydrocarbon potential. Given the costs and technical challenges of exploring deep-water margins this situation is unlikely to change in the near future.

We would like to thank our many colleagues at Liverpool, BP and Badleys who have worked with us on the many studies of continental margins which have contributed directly or indirectly to this paper. Our analysis of rifted margins has evolved through the duration of the iSIMM, MM2 and MM3 research projects and we appreciate the many discussions on margin evolution with our co-investigators for these projects, Bob White, Phil Christie and Gianreto Manatschal. Garry Karner has helped to focus our thoughts on many occasions, not least with his incisive review of our original manuscript. Doug Paton is also thanked for his helpful review. We thank Geoscience Australia for permission to publish the seismic lines in Figures 4 &11 and Brian Horn at ION-GXT for permission to publish the seismic line in Figure 3.

REFERENCES

Alvey, A. 2010. *Using Crustal Thickness and Continental Lithosphere Thinning Factors from Gravity Inversion to Refine Plate Reconstruction Models for the Arctic & North Atlantic*. PhD thesis, University of Liverpool.

Alvey, A., Gaina, C., Kusznir, N.J. & Torsvik, T.H. 2008. Integrated crustal thickness mapping and plate reconstructions for the high Arctic. *Earth and Planetary Science Letters*, **274**, 310–321, http://dx.doi.org/10.1016/j.epsl.2008.07.036.

Baxter, K., Cooper, G.T., Hill, K.C. & O'brien, G.W. 1999. Late Jurassic subsidence and passive margin evolution in the Vulcan Sub-basin, northwest Australia: Constraints from basin modelling. *Basin Research*, **11**, 97–111.

Braun, M.G., Hirth, G. & Parmentier, E.M. 2000. The effects of deep damp melting on mantle flow and melt generation beneath mid-ocean ridges. *Earth and Planetary Science Letters*, **176**, 339–356.

Cannat, M. 1996. How thick is the magmatic crust at slow spreading oceanic ridges? *Journal of Geophysical Research*, **101**, 2847–2857, http://dx.doi.org/10.1029/95JB03116.

Chappell, A.R. & Kusznir, N.J. 2008. Three-dimensional gravity inversion for Moho depth at rifted continental margins incorporating a lithosphere thermal gravity anomaly correction. *Geophysical Journal International*, **174**, 1–13.

Clift, P., Lin, J. & Barckhausen, U. 2002. Evidence of low flexural rigidity and low viscosity lower continental crust during continental break-up in the South China Sea. *Marine and Petroleum Geology*, **19**, 951–970.

Collier, J.S., Minshull, T.A., Hammond, J.O.S. *et al*. 2009. Factors influencing magmatism during continental breakup: New insights from a wide-angle seismic experiment across the conjugate Seychelles–Indian margins. *Journal of Geophysical Research*, **114**, B03101, http://dx.doi.org/10.1029/2008JB005898.

Contrucci, I., Matias, L., Moulin, M. *et al*. 2004. Deep structure of the West African continental margin (Congo, Zaire, Angola), between 58 S and 88 S, from reflection/refraction seismics and gravity data. *Geophysical Journal International*, **158**, 529–553.

Corfield, R.I., Carmichael, S., Bennett, J., Akhter, S., Fatimi, M. & Craig, T. 2010. Variability in the crustal structure of the West Indian Continental Margin in the Northern Arabian Sea. *Petroleum Geoscience*, **16**, 257–265, http://dx.doi.org/10.1144/1354-079309-902.

Cowie, L. & Kusznir, N.J. 2012. Gravity inversion mapping of crustal thickness and lithosphere thinning for the eastern Mediterranean. *The Leading Edge*, July, 810–814.

Daley, T. & Alam, Z. 2002. Seismic stratigraphy of the offshore Indus Basin. *In*: Clift, P.D., Kroon, D., Gaedicke, C. & Craig, J. (eds) *The Tectonic and Climatic Evolution of the Arabian Sea Region*. Geological Society, London, Special Publications, **195**, 259–271, http://dx.doi.org/10.1144/GSL.SP.2002.195.01.14.

Davis, M. & Kusznir, N.J. 2004. Depth-dependent lithospheric stretching at rifted continental margins. *In*: Karner, G.D. (ed.) *Proceedings of NSF Rifted Margins Theoretical Institute*. Columbia University Press, 92–136.

Davison, I. 1999. Tectonics and hydrocarbon distribution along the Brazilian South Atlantic margin. *In*: Cameron, N.R., Bate, R.H. & Clure, V.S. (eds) *The Oil and Gas Habitats of the South Atlantic*. Geological Society, London, Special Publications, **153**, 133–151, http://dx.doi.org/10.1144/GSL.SP.1999.153.01.09.

Divins, D.L. 2009. NGDC Total Sediment Thickness of the World's Oceans & Marginal Seas, http://www.ngdc.noaa.gov/mgg/sedthick/sedthick.html.

Driscoll, N.W. & Karner, G.D. 1998. Lower crustal extension across the Northern Carnarvon Basin, Australia: Evidence for an eastward dipping detachment. *Journal of Geophysical Research*, **103**, 4975–4991.

Eccles, J.D., White, R.S. & Christie, P.A.F. 2011. The composition and structure of volcanic rifted continental margins in the North Atlantic: Further insight from shear waves. *Tectonophysics*, **508**, 22–33, http://dx.doi.org/10.1016/j.tecto.2010.02.001.

Farr, T.G., Rosen, P.A. & Caro, E. and 15 others. 2007. The shuttle radar topography mission: *Reviews of Geophysics*, **45** (2), RG2004, http://dx.doi.org/10.1029/2005RG000183.

Fletcher, R.F. 2009. *Mechanisms of Continental Lithosphere Thinning and Rifted Margin Formation*. PhD thesis, University of Liverpool.

Fletcher, R.F., Kusznir, N.J., Roberts, A.M. & Hunsdale, R. in press. The formation of a failed continental breakup basin: The Cenozoic development of the Faroe–Shetland Basin. *Basin Research*.

Funck, T., Hopper, J.R., Larsen, H.C., Louden, K.E., Tucholke, B.E. & Holbrook, W.S. 2003. Crustal structure of the ocean–continent transition at Flemish Cap: Seismic refraction results. *Journal of Geophysical Research*, **108**, 2531, http://dx.doi.org/10.1029/2003JB002434.

IOC, IHO, BODC. 2003. *Centenary Edition of GEBCO Digital Atlas, published on CD-ROM on behalf of the Intergovernmental Oceanographic Commission and the International Hydrographic Organization as part of the General Bathymetric Chart of the Oceans*. British Oceanographic Data Centre, Liverpool, UK.

Goncharov, A. 2004. Basement and crustal structure of the Bonaparte and Browse basins, Australian northwest margin. *In*: Ellis, G.K., Baillie, P.W. & Munson, T.J. (eds) *Timor Sea Petroleum Geoscience. Proceedings of the Timor Sea Symposium, Darwin, Northern Territory, June 2003*. Northern Territory Geological Survey Special Publication, **1**, 1–16.

Green, T., Abdullayev, N., Hossack, J., Riley, G. & Roberts, A.M. 2009. Sedimentation and subsidence in the South Caspian Basin, Azerbaijan. *In*: Brunet, M.-F., Wilmsen, M. & Granath, J.W. (eds) *South Caspian to Central Iran Basins*. Geological Society, London, Special Publications, **312**, 241–260, http://dx.doi.org/10.1144/SP312.12.

Greenhalgh, E.E. & Kusznir, N.J. 2007. Evidence for thin oceanic crust on the extinct Aegir Ridge, Norwegian Basin, NE Atlantic derived from satellite gravity inversion. *Geophysical Research Letters*, **34**, L06305, http://dx.doi.org/10.1029/2007GL02944.

Hoffman, N. & Hill, K.C. 2004. Structural-stratigraphic evolution and hydrocarbon prospectivity of the deep-water Browse Basin, North West Shelf, Australia. *In*: Ellis, G.K., Baillie, P.W. & Munson, T.J. (eds) *Timor Sea Petroleum Geoscience. Proceedings of the Timor Sea Symposium, Darwin, Northern Territory, June 2003*. Northern Territory Geological Survey Special Publication, **1**, 393–409.

Hopper, J.R., Funck, T. & Tucholke, B.E. 2007. Structure of the Flemish Cap margin, Newfoundland: Insights into mantle and crustal processes during continental breakup. *In*: Karner, G.D., Manatschal, G. & Pinheiro, L.M. (eds) *Imaging, Mapping, and Modelling Continental Lithosphere Extension and Breakup*. Geological Society, London, Special Publications, **282**, 47–61.

Huismans, R.S. & Beaumont, C. 2008. Complex rifted continental margins explained by dynamical models of depth-dependent lithospheric extension. *Geology*, **36**, 163–166, http://dx.doi.org/10.1130/G24231A.1.

Huismans, R.S. & Beaumont, C. 2011. Depth-dependent extension, two-stage breakup and cratonic underplating at rifted margins. *Nature*, **473**, 74–79, http://dx.doi.org/10.1038/nature09988.

Karner, G.D. & Driscoll, N.W. 1999*a*. Tectonic and stratigraphic development of the West African and eastern Brazilian Margins: Insights from quantitative basin modelling. *In*: Cameron, N.R., Bate, R.H. & Clure, V.S. (eds) *The Oil and Gas Habitats of the South Atlantic*. Geological Society, London, Special Publications, **153**, 11–40.

Karner, G.D. & Driscoll, N.W. 1999*b*. Style, timing. and distribution of tectonic deformation across the Exmouth Plateau, northwest Australia, determined from stratal architecture and quantitative basin modelling. *In*: Mac Niocaill, C. & Ryan, P.D. (eds) *Continental Tectonics*. Geological Society, London, Special Publications, **164**, 271–311.

Karner, G.D., Driscoll, N.W. & Barker, D.H.N. 2003. Syn-rift regional subsidence across the West African continental margin: The role of lower plate ductile extension. *In*: Arthur, T., Macgregor, D. & Cameron, N.R. (eds) *Petroleum Systems and Evolving Technologies in African Exploration and Production*. Geological Society, London, Special Publications, **207**, 105–129.

Krishna, K.S., Gopalarao, D. & Sar, D. 2006. Nature of the crust in the Laxmi Basin (14°–20°N), western continental margin of India. *Tectonics*, **25**, TC1006, http://dx.doi.org/10.1029/2004TC001747.

Kusznir, N.J. & Karner, G.D. 2007. Continental lithospheric thinning and breakup in response to upwelling divergent mantle flow: Application to the Woodlark, Newfoundland, and Iberia Margins. *In*: Karner, G.D., Manatschal, G. & Pinheiro, L.M. (eds) *Imaging, Mapping and Modelling Continental Lithosphere Extension and Breakup*. Geological Society, London, Special Publications, **282**, 389–419.

Kusznir, N.J., Marsden, G. & Egan, S.S. 1991. A flexural cantilever simple-shear/pure-shear model of continental extension. *In*: Roberts, A.M., Yielding, G. & Freeman, B. (eds) *The Geometry of Normal Faults*. Geological Society, London, Special Publications, **56**, 41–61.

Kusznir, N.J., Roberts, A.M. & Morley, C. 1995. Forward and reverse modelling of rift basin formation. *In*: Lambiase, J. (ed.) *Hydrocarbon Habitat in Rift Basins*. Geological Society, London, Special Publications, **80**, 33–56.

Kusznir, N.J., Hunsdale, R. & Roberts, A.M. 2004. Timing of depth-dependent stretching on the S. Lofoten rifted margin Mid-Norway: Pre-breakup or post-breakup? *Basin Research*, **16**, 279–296.

Kusznir, N.J., Hunsdale, R. & Roberts, A.M. & iSIMM Team. 2005. Timing and magnitude of depth-dependent lithosphere stretching on the southern Lofoten and northern Vøring continental margins offshore mid-Norway: Implications for subsidence and hydrocarbon maturation at volcanic rifted margins. *In*: Doré, A.G. & Vining, B.A. (eds) *Petroleum Geology: North-West Europe & Global Perspectives — Proceedings of the 6th Petroleum Geology Conference*. Geological Society, London, 767–783.

Magnavita, L., Davison, I. & Kusznir, N.J. 1994. The erosion and exhumation history of the Reconcavo-Tucano-Jatoba Rift, N.E. Brazil during south Atlantic opening. *Tectonics*, **13**, 367–388.

Manatschal, G., Müntener, O., Lavier, L.L., Minshull, T.A. & Péron-Pinvidic, G. 2007. Observations from the Alpine Tethys and Iberia–Newfoundland

margins pertinent to the interpretation of continental breakup. *In*: Karner, G.D., Manatschal, G. & Pinheiro, L.M. (eds) *Imaging, Mapping and Modelling Continental Lithosphere Extension and Breakup*. Geological Society, London, Special Publications, **282**, 291–324, http://dx.doi.org/10.1144/SP282.14.

Marsden, G., Yielding, G., Roberts, A.M. & Kusznir, N.J. 1990. Application of a flexural cantilever simple-shear/pure-shear model of continental lithosphere extension to the formation of the North Sea. *In*: Blundell, D.J. & Gibbs, A.D. (eds) *Tectonic Evolution of the North Sea Rifts*. Oxford University Press, New York, 241–261.

McKenzie, D.P. 1978. Some remarks on the development of sedimentary basins. *Earth and Planetary Science Letters*, **40**, 25–32.

McKenzie, D.P. & Bickle, M.J. 1988. The volume and composition of melt generated by extension of the lithosphere. *Journal of Petrology*, **29**, 625–679.

Mohriak, W., Nemcok, M. & Enciso, G. 2008. South Atlantic divergent margin evolution: Rift-border uplift and salt tectonics in the basins of SE Brazil. *In*: Pankhurst, R.J., Trouw, R.A.J., Britoneves, B.B. & De Wit, M.J. (eds) *West Gondwana: Pre-Cenozoic Correlations Across the South Atlantic Region*. Geological Society, London, Special Publications, **294**, 365–398, http://dx.doi.org/10.1144/SP294.19.

Nielsen, T.K. & Hopper, J.R. 2004. From rift to drift: Mantle melting during continental breakup. *Geochemistry Geophysics Geosystems*, **5**, Q07003, http://dx.doi.org/10.1029/2003GC000662.

Reston, T. 2007. Extension discrepancy at North Atlantic nonvolcanic rifted margins: depth-dependent stretching or unrecognized faulting. *Geology*, **35**, 367–370, http://dx.doi.org/10.1130/G23213A.1

Roberts, A.M., Yielding, G., Kusznir, N.J., Walker, I. & Dorn Lopez, D. 1993. Mesozoic extension in the North Sea: Constraints from flexural backstripping, forward modelling and fault populations. *In*: Parker, J.R. (ed.) *Petroleum Geology of Northwest Europe. Proceedings of the 4th Conference*. Geological Society, London, 1123–1136.

Roberts, A.M., Lundin, E.R. & Kusznir, N.J. 1997. Subsidence of the Vøring Basin and the influence of the Atlantic continental margin. *Journal of the Geological Society, London*, **154**, 551–557.

Roberts, A.M., Kusznir, N.J., Yielding, G. & Styles, P. 1998. 2D flexural backstripping of extensional basins; the need for a sideways glance. *Petroleum Geoscience*, **4**, 327–338.

Roberts, A.M., Goh, L.S., Hooper, R., De-Jong, M. & Veltmeyer, H. 1999. Quantitative analysis of structure and subsidence in the Nam Con Son Basin, offshore Vietnam: Differential stretching ahead of a propagating ocean? *American Association of Petroleum Geologists Bulletin*, **83**, 1336.

Roberts, A.M., Corfield, R.I., Kusznir, N.J., Matthews, S.J., Kåre-Hansen, E. & Hooper, R.J. 2009. Mapping palaeostructure and palaeobathymetry along the Norwegian Atlantic continental margin: Møre and Vøring Basins. *Petroleum Geoscience*, **15**, 27–43, http://dx.doi.org/10.1144/1354-079309-804.

Roberts, G. 2008. Deepwater West Coast India – The Opening Up of a New Play. *GEO ExPro*, **5**, 52–58.

Royden, L. & Keen, C.E. 1980. Rifting process and thermal evolution of the continental margin of eastern Canada determined from subsidence curves. *Earth and Planetary Science Letters*, **51**, 343–356.

Sandwell, D.T. & Smith, W.H.F. 1997. Marine gravity anomaly from Geosat and ERS-1 satellite altimetry. *Journal of Geophysical Research*, **102**, 10 039–10 054.

Sandwell, D.T. & Smith, W.H.F. 2009. Global marine gravity from retracked Geosat and ERS-1 altimetry: Ridge Segmentation versus spreading rate. *Journal of Geophysical Research*, **114**, B01411, http://dx.doi.org/10.1029/2008JB006008.

Scotchman, I.C., Marais-Gilchrist, G., deSouza, F.G., Chaves, F.F., Atterton, L.A., Roberts, A.M. & Kusznir, N.J. 2006. A failed sea-floor spreading centre, Santos Basin, Brasil. Rio Oil & Gas Expo and Conference 2006 Annals. Instituto Brasileiro de Petroleo e Gas, Rio de Janeiro.

Scotchman, I.C., Gilchrist, G., Kusznir, N.J., Roberts, A.M. & Fletcher, R. 2010. The breakup of the South Atlantic Ocean: formation of failed spreading axes and blocks of thinned continental crust in the Santos Basin, Brazil and its consequences for petroleum system development. *In*: Vining, B.A. & Pickering, S.C. (eds) *Petroleum Geology: From Mature Basins to New Frontiers - Proceedings of the 7th Petroleum Geology Conference*. Geological Society, London, 855–866, http://dx.doi.org/10.11444/0070855

Shillington, D.J., Scott, C.L., Minshull, T.A., Edwards, R.A., Brown, P.J. & White, N.J. 2009. Abrupt transition from magma-starved to magma-rich rifting in the eastern Black Sea. *Geology*, **37**, 7–10.

Spiegelman, M. & Reynolds, J.R. 1999. Combined dynamic and geochemical evidence for convergent melt flow beneath the East Pacific Rise. *Nature*, **402**, 282–285.

Struckmeyer, H.I.M., Blevin, J.E., Sayers, J., Totterdell, J.M., Baxter, K. & Cathro, D.L. 1998. Structural evolution of the Browse Basin. North West Shelf. new concepts from deep seismic data. *In*: Purcell, P.G. & Purcell, R.R. (eds) *The Sedimentary Basins of Western Australia 2: Proceedings of the Petroleum Exploration Society of Australia Symposium*. Perth, WA, 345–367.

Symonds, P.A., Collins, C.D.N. & Bradshaw, J. 1994. Deep structure of the Browse Basin: Implications for basin development and petroleum exploration. *In*: Purcell, P.G. & Purcell, R.R. (eds) *The Sedimentary Basins of Western Australia. Proceedings of the Petroleum Exploration Society of Australia Symposium*. Perth, WA, 315–331.

Symonds, P.A., Planke, S., Frey, O. & Skogseid, J. 1998. Volcanic evolution of the Western Australian Continental Margin and its implications for basin development. *In*: Purcell, P.G. & Purcell, R.R. (eds) *The Sedimentary Basins of Western Australia 2. Proceedings of the Petroleum Exploration Society of Australia Symposium*. Perth, WA, 33–54.

Talwani, M. & Reif, C. 1998. Laxmi Ridge – A continental sliver in the Arabian Sea. *Marine Geophysical Researches*, **20**, 259–271.

Tucholke, B.E., Sawyer, D.S. & Sibuet, J.-C. 2007. Breakup of the Newfoundland–Iberia rift. *In*: Karner, G.D., Manatschal, G. & Pinheiro, L.M. (eds) *Imaging, Mapping, and Modelling Continental Lithosphere Extension and Breakup*. Geological Society, London, Special Publications, **282**, 9–45.

White, R.S. & McKenzie, D.P. 1989. Magmatism at rift zones: The generation of volcanic continental margins and flood basalts. *Journal of Geophysical Research*, **94**, 7685–7729.

White, R.S. & Smith, L.K. 2009. Crustal structure of the Hatton and the conjugate east Greenland rifted volcanic continental margins, NE Atlantic. *Journal of Geophysical Research*, **114**, B02305, http://dx.doi.org/10.1029/2008JB005856.

Whitmarsh, R.B., Manatschal, G. & Minshull, T.A. 2001. Evolution of magma-poor continental margins from rifting to seafloor spreading. *Nature*, **413**, 150–154, http://dx.doi.org/10.1038/35093085.

Yielding, G. & Roberts, A.M. 1992. Footwall uplift during normal faulting – implications for structural geometries in the North Sea. *In*: Larsen, R.M. *et al.* (eds) *Structural and Tectonic Modelling and its Application to Petroleum Geology*. Norwegian Petroleum Society, Special Publication, **1**, 289–304.

Zelt, C.A., Sain, K., Naumenko, J.V. & Sawyer, D.S. 2003. Assessment of crustal velocity models using seismic refraction and reflection tomography. *Geophysical Journal International*, **153**, 609–626.

Received 15 July 2011; revised typescript accepted 15 October 2012.